2010

Effects of turbulence intensity and integral length scale on an asymmetric airfoil at low Reynolds numbers

Ning Cao
University of Windsor

Effects of turbulence intensity and integral length scale on an asymmetric airfoil at low Reynolds numbers

by

Ning Cao

A Thesis
Submitted to the Faculty of Graduate Studies
through Mechanical, Automotive, and Materials Engineering
in Partial Fulfillment of the Requirements for
the Degree of Master of Applied Science at the
University of Windsor

Windsor, Ontario, Canada

2010

Effects of turbulence intensity and integral length scale on an asymmetric airfoil at low Reynolds numbers

by

Ning Cao

APPROVED BY:

_____

Dr. A. Edrisy, Outside Program Reader
Program of Engineering Materials

_____

Dr. G. Rankin, Program Reader
Department of Mechanical, Automotive and Materials Engineering

_____

Dr. R. Carriveau, Co-Advisor
Department of Civil and Environmental Engineering

_____

Dr. D. S-K. Ting, Co-Advisor
Department of Mechanical, Automotive and Materials Engineering

_____

Dr. N. Zamani, Chair of Defense
Department of Mechanical, Automotive and Materials Engineering

September 17, 2010

DECLARATION OF PREVIOUS PUBLICATION

This thesis includes 2 original papers that have been previously published/submitted for publication in peer reviewed journals, as follows:

Thesis Chapter	Publication title/full citation	Publication status*
Chapter 2	N. Cao, D. S-K. Ting, and R. Carriveau, Effects of turbulence intensity and integral length scale on an airfoil performance, AIAA Journal	Under review
Chapter 3	N. Cao, R. Carriveau, and D. S-K. Ting, The wake structure of a high-lift airfoil under free-stream turbulence with different intensity and length scale, Experimental Thermal and Fluid Science	To be submit

I certify that I have obtained a written permission from the copyright owner(s) to include the above published material(s) in my thesis. I certify that the above material describes work completed during my registration as graduate student at the University of Windsor.

I declare that, to the best of my knowledge, my thesis does not infringe upon anyone's copyright nor violate any proprietary rights and that any ideas, techniques, quotations, or any other material from the work of other people included in my thesis, published or otherwise, are fully acknowledged in accordance with the standard referencing practices. Furthermore, to the extent that I have included copyrighted material that surpasses the bounds of fair dealing within the meaning of the Canada Copyright Act, I certify that I have obtained a written permission from the copyright owner(s) to include such material(s) in my thesis.

I declare that this is a true copy of my thesis, including any final revisions, as approved by my thesis committee and the Graduate Studies office, and that this thesis has not been submitted for a higher degree to any other University or Institution.

ABSTRACT

In the thesis, the performance of an asymmetric, high-lift S1223 airfoil has been investigated at Reynolds numbers 55,000, 75,000, and 100,000. The airfoil was tested in a quasi-isotropic turbulent flow generated using orificed perforated plates. The independent effects of the turbulence intensity were examined at a constant integral length scale. The stall of the airfoil is delayed by increasing the turbulence intensity. The wake of the airfoil becomes narrower and the strength of the shedding vortices was reduced, which indicates a suppression of the boundary layer of the airfoil. The independent roles of integral length scale were examined at turbulence intensity of 4.1% and 9.5%. At Tu=4.1% with increasing the integral length scale, the stall of the airfoil is delayed, and wider wakes have been observed at the stall region. At Tu=9.5%, the effects of turbulence scale become subtle.

DEDICATION

To my parents

ACKNOWLEDGEMENTS

I would like to show my sincere gratitude to Dr. D. S-K. Ting and Dr. R. Carriveau for their guidance and instruction offered throughout this research. I will not forget the moment we spent together discussing issues and problems. I appreciate that they have shown me the true professionalism and determination.

The research would have been impossible without the maximum technical support from Mr. A. Jenner and Mr. P. Seguin. Mr. Jenner provided his help in manufacturing several fixtures that are essential to my research. And Mr. Seguin offered me his extensive knowledge in electronics.

I would like to thank the committee member Dr. G. Rankin and Dr. A. Edrisy who infused their knowledge and insight into this study.

Financial support from the Natural Sciences and Engineering Research Council of Canada (NSERC) and from the University of Windsor is also appreciated.

TABLE OF CONTENTS

LIST OF TABLES

LIST OF FIGURES

NOMENCLATURE

A	planform area
B	bias error
C	chord of the airfoil, m
C_l	coefficient of lift
$C_{l,max}$	maximum coefficient of lift
C_d	coefficient of drag
D	drag, N
d	diameter of the orifice on orificed perforated plate, m
L	lift, N
l	distance from the orificed perforated plate to the leading edge of the airfoil, m
P	precision error
q	free-stream dynamic pressure, Pa
Re	Reynolds number based on chord
T	integral time scale, s
Tu	turbulence intensity
U_{mean}	mean velocity, m/s
u	velocity fluctuation term, m/s
u'	standard deviation of the velocity fluctuation, m/s
W	uncertainty
α	angle of attack, deg
Λ	integral length scale, mm
λ	Taylor microscale, mm
$\rho(\tau)$	temporal auto-correlation coefficient
τ	time, s

CHAPTER 1. INTRODUCTION

Background and Motivation

The behaviour of airfoils operating in turbulence at low Reynolds numbers is critical in many engineering applications including micro air vehicles and small scale wind turbines. These devices usually operate in atmospheric turbulence and the performance of airfoils in turbulence is less stable and harder to predict since many parameters in the oncoming turbulent free-stream have effects on the flow field and the boundary layer of airfoils. Two relatively independent parameters are commonly utilized to offer descriptions of turbulence: turbulence intensity and turbulence integral length scale. As they can be manipulated semi-independently in a controlled laboratory condition, it is possible to have a better understanding of their independent effects on the performance and the wake of the airfoil.

Scope of Study

The study focuses on the independent effects of the turbulence intensity and integral length scale on the performance and the wake of an asymmetric, high-lift S1223 airfoil at different Reynolds numbers.

In chapter 2, the measurement of lift and drag data was carried out under grid turbulence with either constant turbulence intensity or constant turbulence integral length scale. The angle of attack of the airfoil was changed between -5 to 25 degrees, sufficient to cover the pre-stall and post-stall characteristics of the airfoil.

In chapter 3, the wake of the airfoil was surveyed at different turbulence level with its structure examined carefully at pre-stall and post-stall region.

CHAPTER 2. EFFECTS OF TURBULENCE ON THE PERFORMANCE OF THE AIRFOIL

Introduction

The behaviour of airfoils operating in a turbulent free-stream at low Reynolds numbers based on chord (typically less than 200,000) is critical in many engineering applications including micro air vehicles and small scale wind turbines. These devices usually operate in atmospheric turbulence, so the performance of airfoils in turbulence is more difficult to predict since many parameters in the oncoming turbulent free-stream have effects on the flow field and the boundary layer of airfoils. Two relatively independent parameters are commonly utilized to offer descriptions of turbulence: turbulence intensity which represents the level of velocity fluctuation and turbulence integral length scale which is a measure of the size of energy-containing eddies. As they can be manipulated semi-independently in a controlled laboratory condition, it is possible to have a better understanding of their independent effects on the performance of the airfoil, which may also improve the prediction of the performance of the airfoil in atmospheric turbulence. Before the discussion on free-stream turbulence effects on the performance of the airfoil, it is worth describing some of the flow characteristics of the airfoil at low Reynolds number in hopes of providing insight on the effects of free-stream turbulence.

The performance of airfoils at low Reynolds number has been extensively studied and well documented [1-3]. Below a certain critical Reynolds number (approximately 70,000), the laminar boundary layer develops on the suction surface (or lifting surface) of an airfoil. As the angle of attack α increases, the laminar boundary layer separates to form a separated shear layer since it does not have enough energy to overcome the adverse pressure gradient developed on the lifting surface. The separation may occur over the entire rear of the airfoil, and it is unusual for reattachment to occur below the critical Reynolds number [1]. The lift-to-drag ratio is typically low at this stage since the airfoil has low lift and high drag due to the boundary layer separation. As the Reynolds number increases above 70,000, the laminar shear layer experiences faster transition to become turbulent. The turbulent boundary layer contains more energy, so it is better equipped to overcome the adverse pressure gradient. As a consequence, reattachment of the boundary

layer occurs, and a short laminar separation bubble forms. With further increase in α, a larger adverse pressure gradient exerts more pressure on the turbulent boundary layer until a point that the short bubble "bursts", and the boundary layer separates from the suction surface again. The airfoil stalls, and this is characterized by an abrupt loss of lift and a drastic increase in drag. In order to recover the airfoil from stall, the angle of attack needs to be reduced so that the reattachment of the boundary layer is possible. However the boundary layer might not reattach to the airfoil at the same α where the separation occurred; rather, the reattachment process is delayed to a lower α. This phenomenon is known as a hysteresis effect.

An increase in turbulence intensity in the free-stream (without considering the integral length scale effects) has been shown to change the performance of the airfoil which is equivalent to an increase in *Re*, and the hysteresis effect diminishes as the free-stream becomes more turbulent. Mueller et al. [4] discussed the effects of free-stream disturbances on a Lissaman 7769 airfoil with turbulence level up to 0.3% at a Reynolds number around 150,000. They pointed out that an increase in turbulence intensity advances the boundary layer transition point to the leading edge of the airfoil. The significant hysteresis region originally presented at a very low turbulence level (0.08%) was later reduced when turbulence intensity was increased to 0.3% due to the reattachment of the boundary layer at higher angles of attack. Similar effects were observed by Hoffmann [5], who also found that the maximum coefficient of lift of the NACA 0015 airfoil increases 30% as the turbulence intensity goes from 0.25% to 9% at Re=250,000, and the corresponding α required to reach $C_{l,max}$ increases from 21 to 29 deg. The coefficient of drag is increased slightly with turbulence due to an increase in skin friction. Payne and Nelson [6] indicated that turbulence increases the effective Reynolds number of the airfoil in the shear flow, thereby reducing the size of the laminar separation bubble and increasing the lift at a given angle of attack. Devinant et al. [7] also observed that as the turbulence level of the external flow is increased, a pronounced slowdown of the upstream advance of separation point occurs with a major increase in $C_{l,max}$. The high turbulence level increases the energy transfer between the external flow and the boundary layer, which has the effect of increasing its resistance to separation. Overall, free-stream turbulence improves the C_l of an airfoil by influencing its boundary layer.

However, turbulence intensity and turbulence integral length scale can be perceived independent from each other: two different turbulent flows may have the same turbulence intensity but differ in turbulence integral length scale, or vice versa. The integral length scale alone has been shown to influence the boundary layer of flat plates and airfoils. Meier and Kreplin [8] evaluated the drag coefficient on a flat plate subjected to different free-stream turbulence structures. The turbulence intensity was held constant at approximately 0.2% with a free-stream velocity of 20 m/s. By varying the turbulence structure, the maximum friction coefficient is obtained as the integral length scale is on the order of the boundary layer thickness. They predicted that a drastic increase of the length scale should no longer affect the boundary layer development at low turbulence intensity (Tu<0.2%). Howard and Kindelspire [9] stated the importance of the length scale on the boundary layer of an airfoil: in order to let the free-stream turbulence to affect the turbulent boundary-layer behaviour, the length scale must be on the order of the boundary-layer thickness. In a paper describing the integral length scale effect on the heat transfer of a circular cylinder, Sak et al. [10] indicated that the decrease of the length scale at constant turbulence intensity results an increase in the heat transfer rate. Among current literature, little has been addressed on the independent role of these turbulence parameters on the performance of the airfoil. However, it can be reasonably argued that the turbulence integral length scale can affect the performance of an airfoil in free-stream turbulence based on its impact on the boundary layer and possibly on the near wake as well.

The current study focuses on the independent effects of the turbulence intensity and integral length scale on the performance, namely C_l and C_d, of an asymmetric, high-lift airfoil, at different Re, in hopes of differentiating their independent effects.

Experimental Methods

Wind Tunnel

The experiment was carried out in a closed-loop wind tunnel with a contraction ratio of 5.76:1. The test section is nominally 4 m long, 0.762 m high by 0.762 m wide. The height of the test section expands gradually to 0.787 m where the airfoil was located.

The wind tunnel can provide steady and uniform flow between 3 m/s and 20 m/s with the test section empty and the turbulence level around 0.5%.

The free-stream speed was checked by a pitot-static tube positioned at the center of the test section. Once the experiment started, the pitot tube was removed from the wind tunnel to prevent its interference with the flow.

Airfoil Model

A S1223 [11] high-lift asymmetric airfoil as shown in Fig. 2.1, made of wood, was used in the experiment. This airfoil could be a very desirable candidate for micro air vehicles and wind turbine applications for its high-lift, low-drag characteristics at low Reynolds numbers. The chord length of the airfoil was 0.1524 m (6 in) with a span-to-chord ratio of 5.0. The airfoil was painted in white and then covered by layers of clear acrylic paint. The surface was finally buffered by using NOVUS plastic polish No.2 to improve its smoothness.

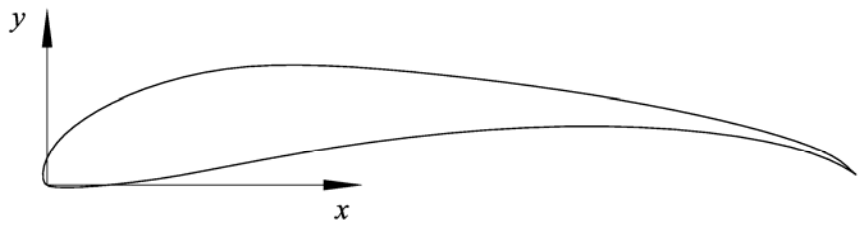

Fig. 2.1 High lift asymmetric S1223 airfoil geometry.

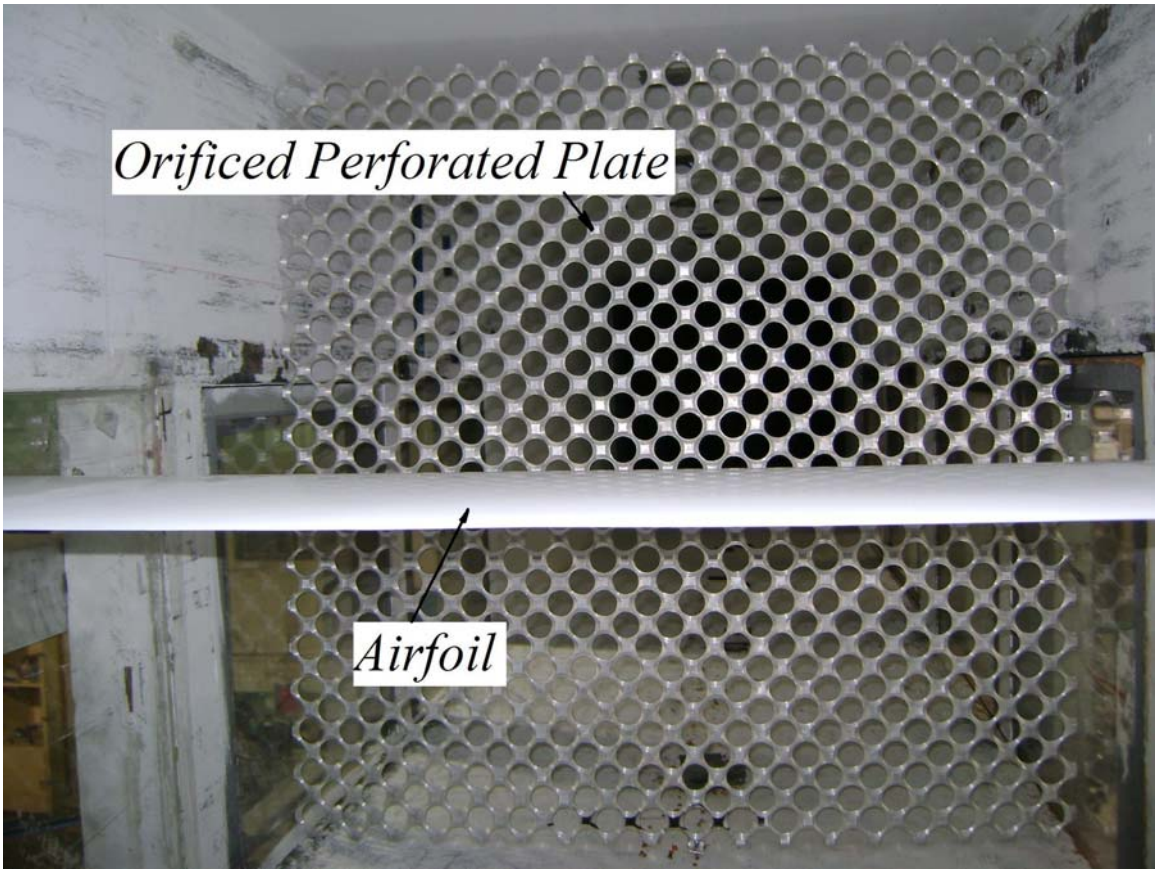

Fig. 2.2 Wind tunnel setup looking upstream.

Force Measurement

The airfoil was located 0.394 m above the floor of the wind tunnel and 3.33 m downstream of the inlet of the test section. The setup is shown in Fig. 2.2. A custom made force/torque measuring platform was built for the study. The airfoil was supported by two transducer fixture sets at its ends through supporting rods that were inserted into the airfoil and were secured by set screws. Looking downstream, the supporting rod at right-side (Fig. 2.3) was connected to a swivel bearing inside of a mounting plate that was fastened to the transducer. The airfoil can rotate freely while the force transducer remained stationary. The airfoil was supported by a radial ball bearing at the left-side fixture (Fig. 2.4). Two set screws were added to fix the desired angle of attack. A protractor indicated the angle of attack with accuracy estimated to be +/-0.3 deg. The fixtures were clamped to aluminium angles mounted outside of the wind tunnel.

Two ATI Gamma type six-component strain force/torque transducers were utilized in this experiment. The maximum force measuring range of one transducer was

+/-65N with a resolution of 1/80 N (0.0125 N). It was mounted on the right-side when looking downstream. The other force/torque transducer, with +/-32N range and a resolution of 1/160 N (0.00625 N), was mounted at the left-side, and the range of torque was 2.5 N-m with a resolution of 1/2000 N-m. The transducers were carefully positioned before the experiment so that the x-axis was parallel to the direction of flow, and the positive y-axis was pointing up perpendicularly. The tilting angle was less than 0.3 deg. The lift was calculated by the summation of the force components in y-direction from the two load cells, and the drag was the summation of the force components in x-direction. The sampling frequency was 1 kHz, and at least 20,000 samples were recorded at each angle of attack. The overall uncertainty of the lift and drag coefficient was estimated to be less than 5%.

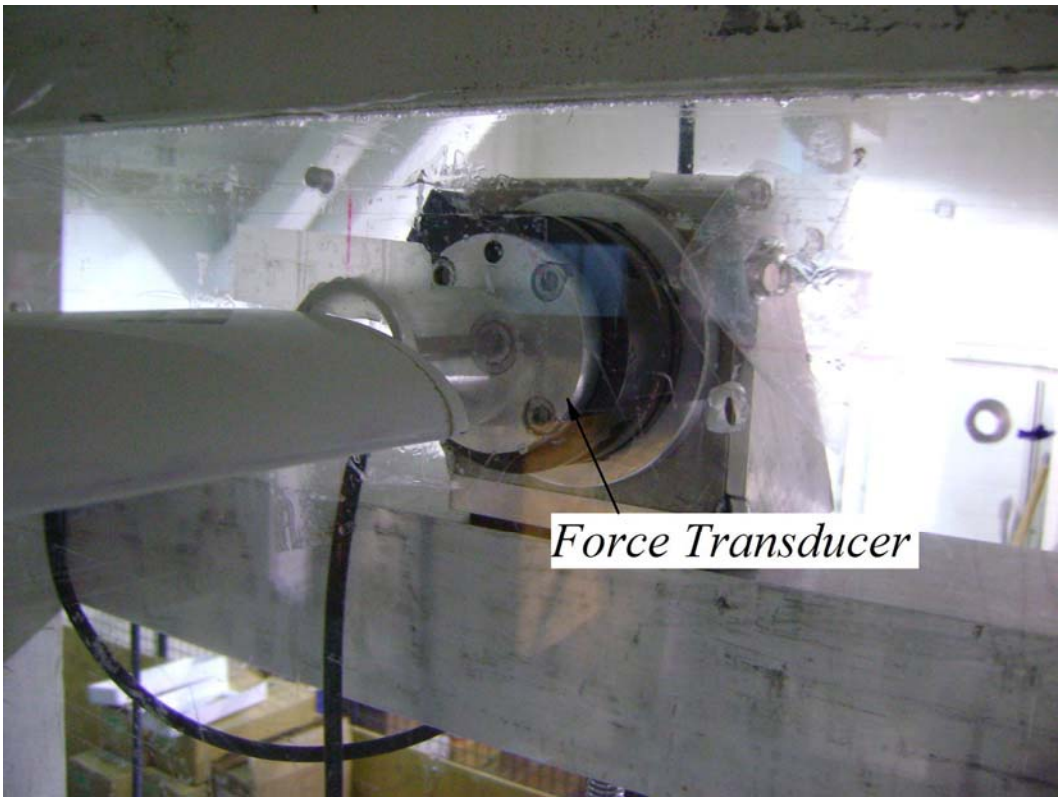

Fig. 2.3 Detail of the right-side fixture looking downstream.

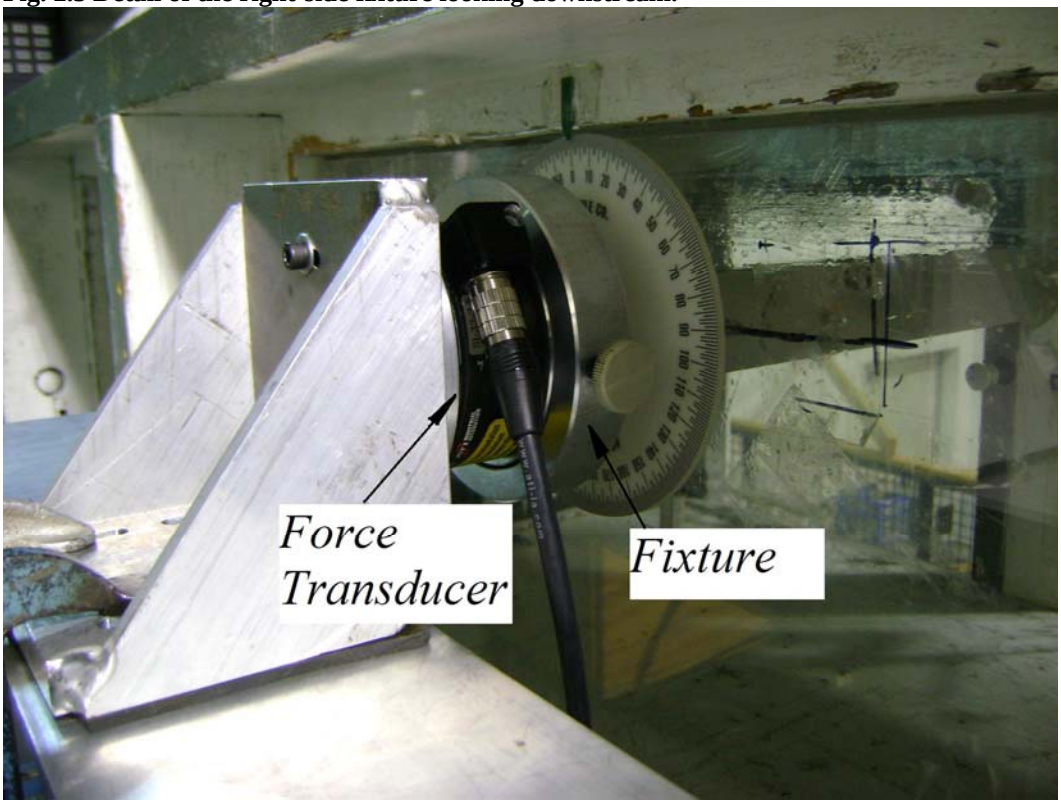

Fig. 2.4 Detail of the left-side fixture looking downstream.

Turbulence Generation

Specially constructed orificed perforated plates [12, 13] were utilized for turbulence generation. The plates were fabricated by drilling a matrix of orificed holes on a 3 mm-thick aluminium sheet (shown in Fig. 2.5). Each hole had a chamfer of 41˚, and the sharp-edge side faced the incoming flow. The sharp-edged design reduces the thickness effect of the plate on the turbulence structure. It provides a better quasi-isotropic turbulent flow compared to conventional solid-bar turbulence generation grids [13].

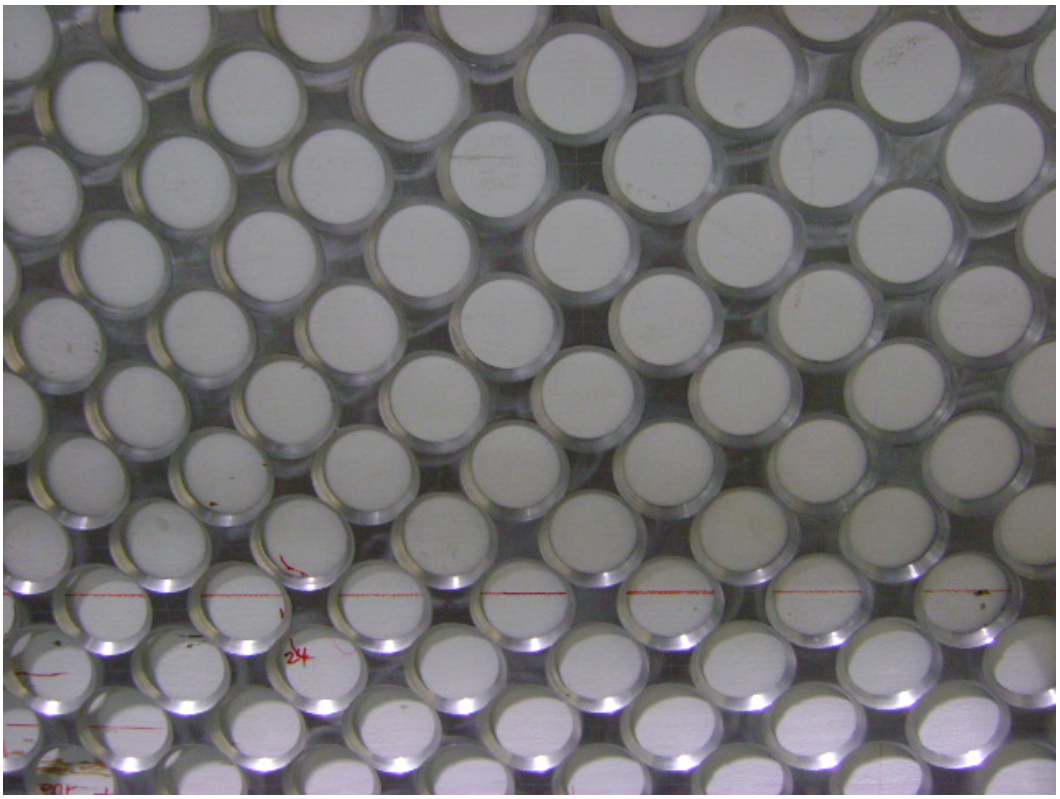

Fig. 2.5 A sample of orificed perforated plate used to generate different levels of turbulence.

Turbulence parameters were calculated from instantaneous velocity data measured using a Dantec streamline 55C90 constant temperature anemometer with a Dantec Type 55P01 single-wire gold-plated probe. The analog voltage signal was first low-passed at 30 kHz using an analog filter to avoid aliasing, and then it was sampled at 80 kHz over 125 s period through a 12 bit PCI-6071E National Instrument data acquisition card. The free-stream turbulence was quantified in the absence of the airfoil with the hot-wire wire anemometer placed at the center of the cross plane where the

leading edge of the airfoil were to be located. The integral length scale is approximated by Taylor's frozen eddy hypothesis, and it is determined as:

$$\Lambda = T \times U_{mean} \tag{2-1}$$

where U_{mean} is the mean airflow velocity, and T is the integral time scale found by:

$$T = \int f(\tau) d\tau \tag{2-2}$$

where f is the auto-correlation function of time:

$$f(\tau) = \frac{1}{u'^2} \int u(t) u(t-\tau) dt \tag{2-3}$$

The autocorrelation function $f(\tau)$ shown in Eq (2-4) can be calculated numerically as follows:

$$f(m\Delta t) = \frac{\frac{1}{N-m} \sum_{i=1}^{N-m} u_i u_{i+m}}{\frac{1}{N} \sum_{i=1}^{N} u_i^2} \qquad 0 < m < N-1 \tag{2-4}$$

where N is total number of samples. The integral time scale was deduced as:

$$T = (\sum_{i=0}^{N-1} f(i)) \Delta t \tag{2-5}$$

Multiple-tests method [14] was followed to determine the uncertainty of turbulence parameters. Turbulence intensity and integral length scale were directly calculated from the velocity fluctuation data for each test, and ten runs were executed. The mean and the standard deviation of the turbulence parameters of the ten runs were calculated. Student t-distribution of 9-degrees of freedom was used to find the uncertainty. Largest value of uncertainties was selected to describe the overall uncertainty level. The turbulence parameters and their uncertainties are listed in Table 2.1.

Table 2.1 Turbulence parameter generated by orificed perforated plated

	d [m]	l[m]	l/d	Mean Tu	Uncertainty Tu	Mean Λ [mm]	Uncertainty Λ [mm]
Plate 25.4	0.0254	0.318	12.5	9.5%	+/-0.2%	12	3.8
Plate 25.4	0.0254	0.889	35.0	4.1%	+/-0.2%	21	3.8
Plate 50.8	0.0508	0.629	12.4	9.5%	+/-0.2%	22	3.8
Plate 50.8	0.0508	1.778	35.0	4.1%	+/-0.2%	35	3.8

At Tu=4.1%, turbulence intensity decreases over the length of the airfoil cord (c=152.4 mm) from 4.1% to 3.6% for the Λ/c=0.14 (Λ=21 mm) case, and from 4.1% to 3.9% for the Λ/c=0.23 (Λ=35 mm) case. The decaying of the turbulence intensity over the length of the chord could be considered negligible. While at high turbulence intensity Tu=9.5%, the turbulence decays over the length of the airfoil cord from 9.5% to 6.5% with Λ/c=0.08 (Λ=12 mm), and from 9.5% to 7.5% with Λ/c=0.14 (Λ=22 mm), so these different rates of decaying could potentially affect the results and will be discussed later.

Results and Discussion

Force data were collected as the angle of attack was increased from -5 to 25 deg and then decreased back to 0 deg to record any hysteresis effect. Three Reynolds numbers of Re=55,000, 75,000, and 100,000 were chosen for the testing as the maximum Reynolds number could not exceed 100,000 for the current wind tunnel condition. The independent roles of turbulence intensity were examined by maintaining Re and Λ at relatively the same magnitude. To investigate the independent role of the integral length scale for each Re, the turbulence intensity was kept at either Tu=4.1% or 9.5%. The integral length scale was varied from Λ/c=0.14 to 0.23 (Λ=22 to 35 mm) at Tu=4.1%. At Tu=9.5%, the integral length scale was made to increase from Λ/c=0.08 to 0.14 (Λ=12 to 22 mm) as it was challenging to generate Λ/c>0.23 at this turbulence level in the facility utilized. Coefficients of lift and drag were plotted as a function of the angle of attack. The

following discussion of the results highlights some important observations for each case studied.

Turbulence intensity effect with constant integral length scale

The data on lift and drag were compared with an integral length scale around Λ/c=0.14 in order to examine the independent effects of turbulence intensity (Fig. 2.6). Fig. 2.6a shows the lift and drag curve at *Re*=55,000. As the turbulence intensity increases from 4.1% to 9.5%, no large changes in C_l, and $C_{l,max}$ are detected when α<16. The differences among lift and drag curve are obvious when α is between 16 and 20 deg. At *Tu*=4.1% with Λ/c=0.14, the coefficient of lift drops significantly at α=17 deg, and there exists a sudden rise of C_d indicating an immediate stall of the airfoil. Noticeable hysteresis is also observed as α decreases from 19 deg. While at turbulence intensity *Tu*= 9.5% with Λ/c=0.14, the lift and drag curves do not feature a steep stall, and hysteresis almost diminishes. At all Reynolds number tested, the coefficient of lift and its slope, in general, are observed to be marginally higher at the lower turbulence intensity (*Tu*=4.1%), and this is especially obvious at *Re*=55,000 and *Re*=100,000.

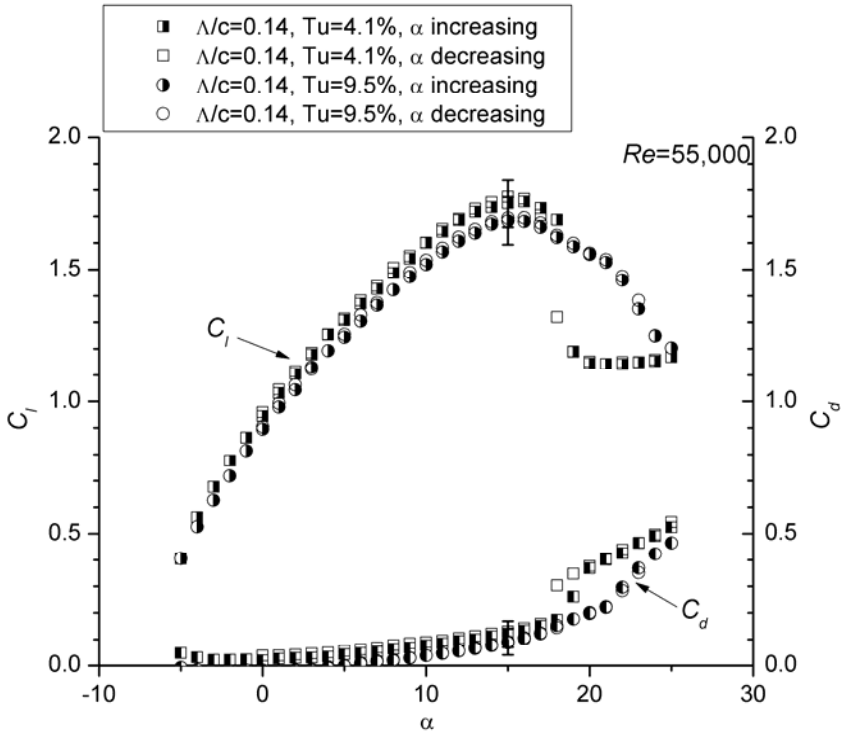

a)

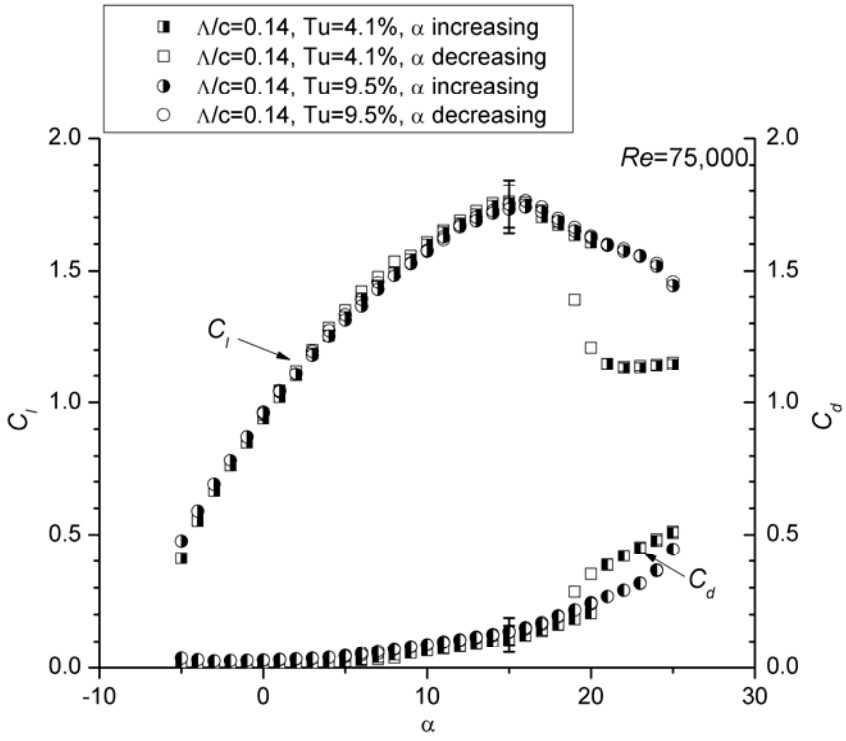

b)

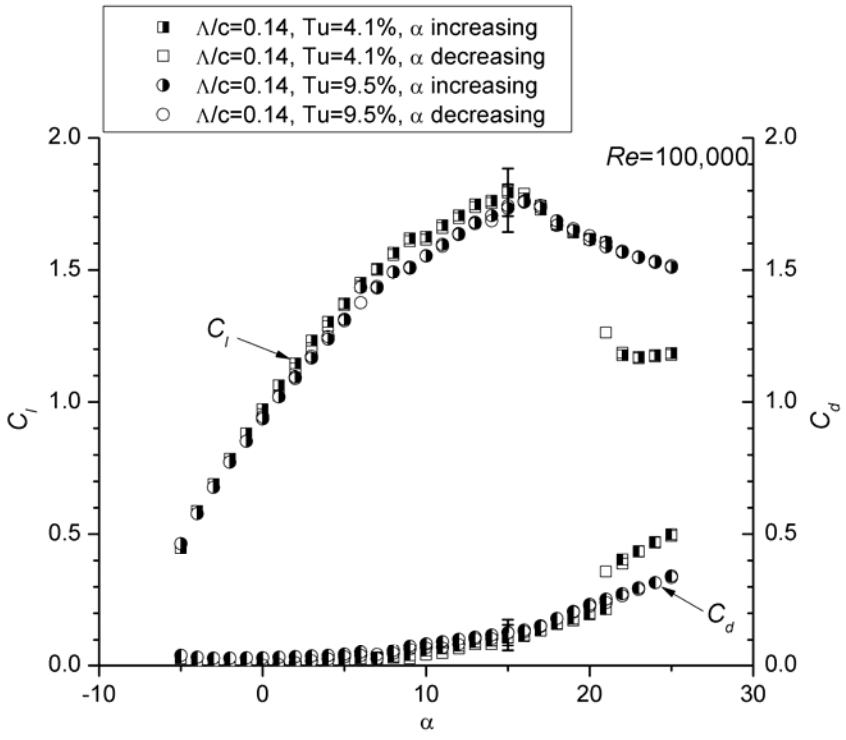

c)

Fig. 2.6 Comparison of coefficient of lift and drag at around *Λ/c*= 0.14, with *Tu*=4.1% and *Tu*=9.5%. a) *Re*=55,000, b) *Re*=75,000, c) *Re*=100,000.

The turbulence intensity alone, with fixed integral length scale, can be said to have great influence on the boundary layer. The boundary layer under the free-stream

with high turbulence intensity, carrying more energy, is more resistant to the strong adverse pressure gradient developed around the aft section of the airfoil, thus preventing or delaying the boundary layer separation at high angle of attack. The airfoil has better stall characteristics when the free-stream turbulence intensity is high. No improvement in $C_{l,max}$ is observed when turbulence intensity is increased at a relatively high level from 4.1 to 9.5%, which seems to be different from the result from Hoffman [5]. However, it should be noted that the turbulence intensity ranged from 0.25% to 9% in Hoffman's experiment, and the 30% increase of $C_{l,max}$ for Tu= 9% is due to the much delayed boundary layer separation at high α. Based on current range of turbulence intensity, we believe its influence on the $C_{l,max}$ to be subtle. The increase of the turbulence intensity also diminishes the hysteresis, which generally agrees what has been observed by Mueller et al. [4], even though the turbulence intensity is much higher in the current experiment.

Integral length scale effect for different turbulence intensity

By comparing the coefficients of lift and drag curves shown in Fig. 2.7 and Fig. 2.8, it is clear that the effects of the integral length scale are largely dependent on the level of turbulence intensity of the free-stream. At low turbulence level Tu=4.1%, the lift curves for both cases exhibit distinct differences. For Re=55,000 with Λ/c=0.14 (Fig. 2.7a), the maximum coefficient of lift is reached at α=16 deg. As the angle of attack continues to increase, the coefficient of lift starts to decrease slightly. The sudden drop of C_l from 1.69 to 1.19 occurs at around α=19 deg with. An abrupt increase of C_d is observed as well. At the larger integral length scale of Λ/c=0.23, the coefficient of lift reaches the peak at a lower α of 15 deg and beyond which it starts to drop rapidly. The coefficients of lift and drag converge to reach the same level at α=19 deg for both cases. When Re is increased to 75,000 and 100,000 (Fig. 2.7b and Fig. 2.7c), the lift and drag curves show similar phenomena as observed previously for Re=55,000: the airfoil tends to stall consistently earlier with a larger free-stream integral length scale, and this is particularly prominent at larger Reynolds number. Small hysteresis is observed with the larger integral scale Λ/c=0.23.

The airfoil does not feature a strong stall characteristic when Λ/c= 0.14. But when Λ/c=0.23, the airfoil stalled immediately after reaching maximum lift. A decrease in C_l

after reaching $C_{l,max}$ is a sign of the separation of the boundary layer, and the decreasing rate of C_l indicates the rate of advancement of the separation point towards the leading edge. It is believed that the smaller size of the energy-containing eddy increase the momentum exchange between outer flow and the boundary layer, adding capacity to overcome the strong adverse pressure gradient and delaying the boundary layer separation near the rear part of the airfoil for high angles of attack. While large eddies marginally help C_l to reach higher values, but the boundary layer lacks the energy to remain attached to the airfoil. Once the separation occurs, the separation point moves quickly towards the leading edge with increasing α.

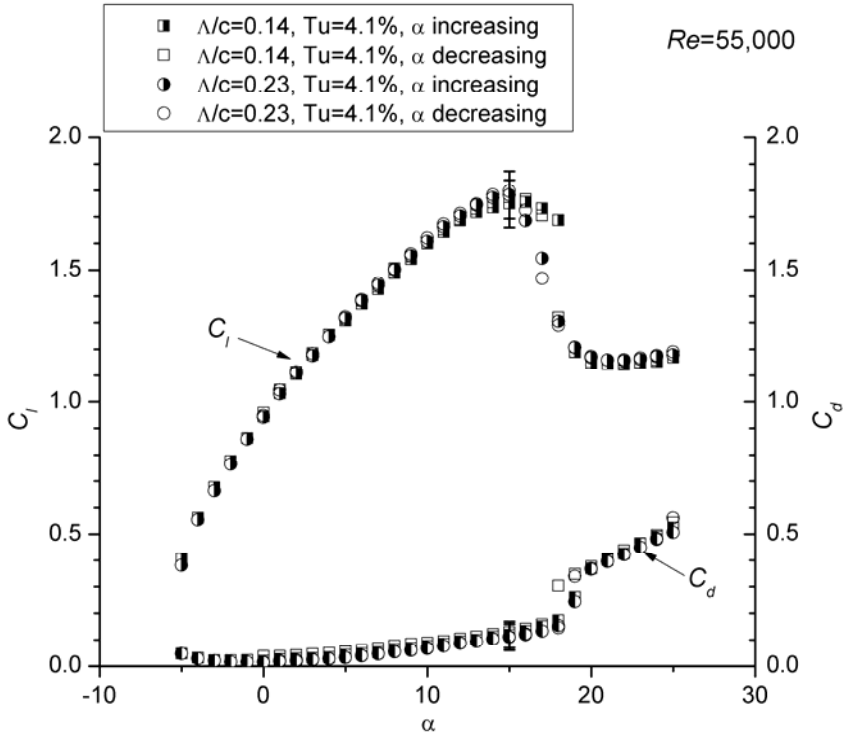

a)

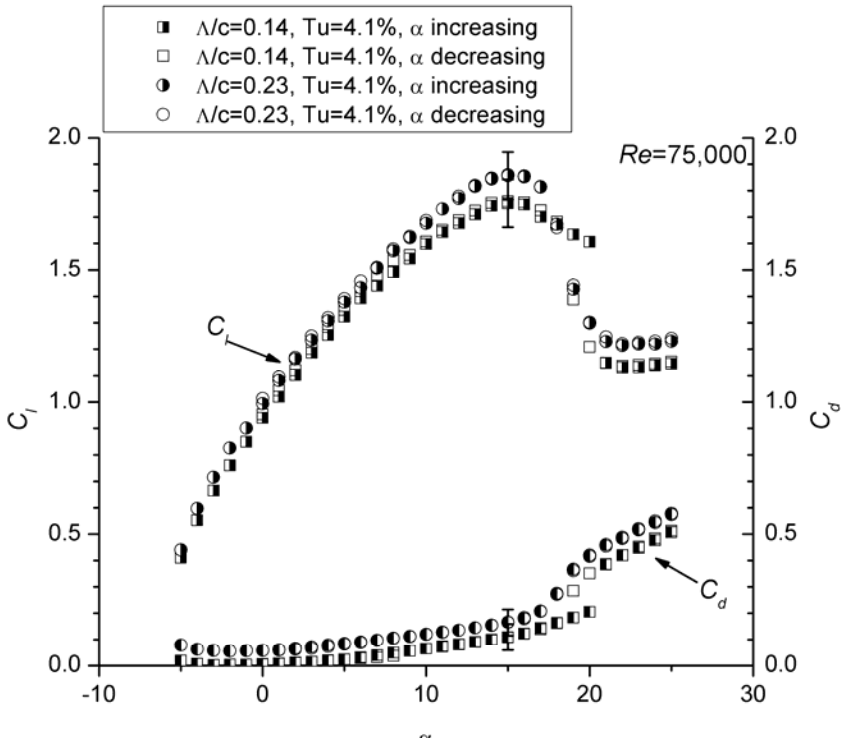

b)

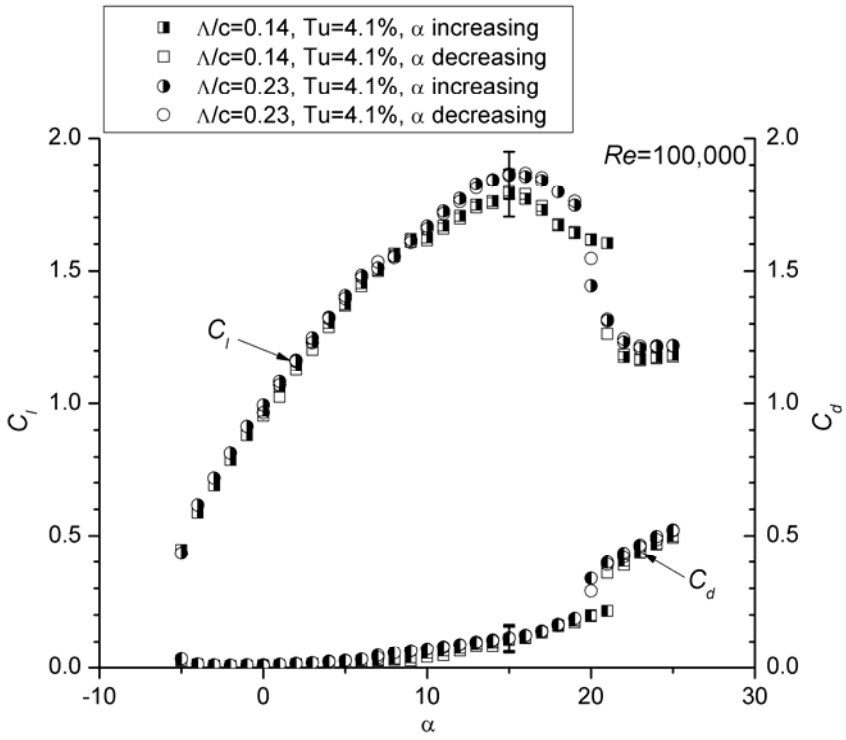

c)

Fig. 2.7 Comparison of coefficient of lift and drag at constant *Tu*=4.1%, with *Λ/c*=0.14 and *Λ/c*=0.23. a) *Re*=55,000, b) *Re*=75,000, c) *Re*=100,000.

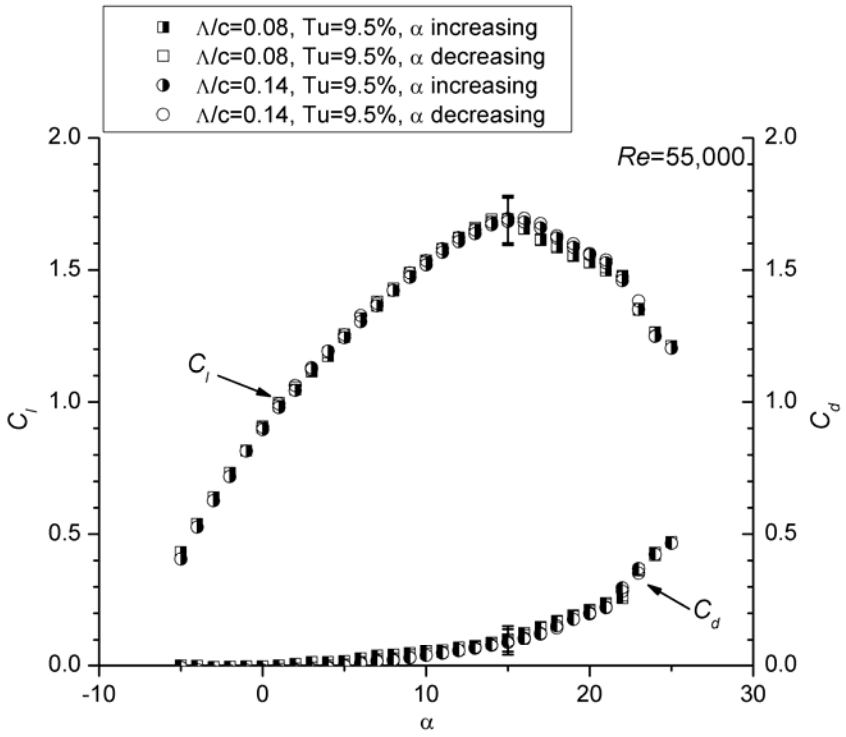
Λ/c=0.08, Tu=9.5%, α increasing
Λ/c=0.08, Tu=9.5%, α decreasing
Λ/c=0.14, Tu=9.5%, α increasing
Λ/c=0.14, Tu=9.5%, α decreasing
Re=55,000
C_l
C_d
α

a)

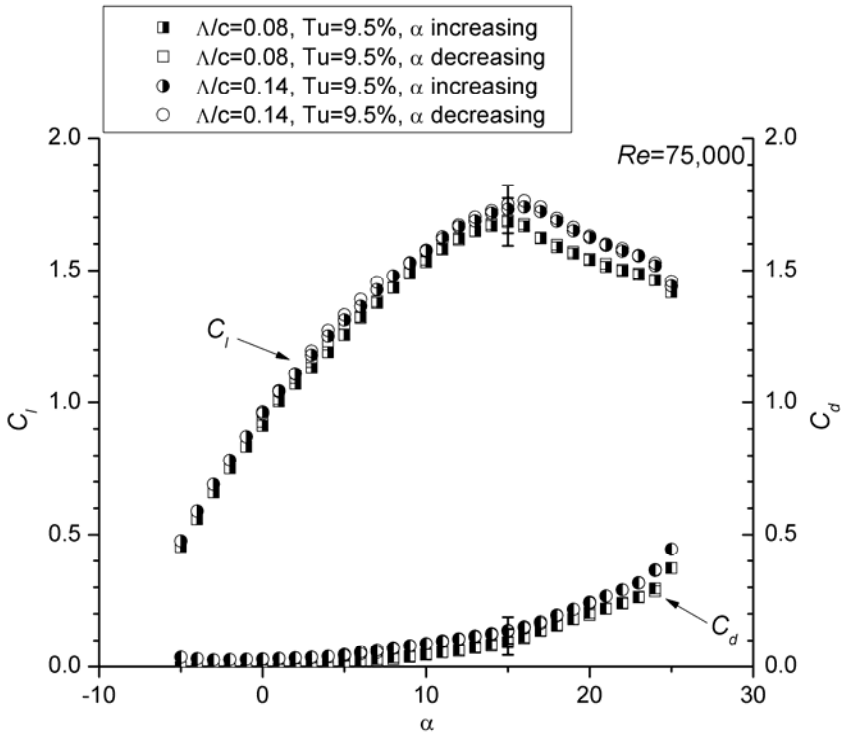
Λ/c=0.08, Tu=9.5%, α increasing
Λ/c=0.08, Tu=9.5%, α decreasing
Λ/c=0.14, Tu=9.5%, α increasing
Λ/c=0.14, Tu=9.5%, α decreasing
Re=75,000
C_l
C_d
α

b)

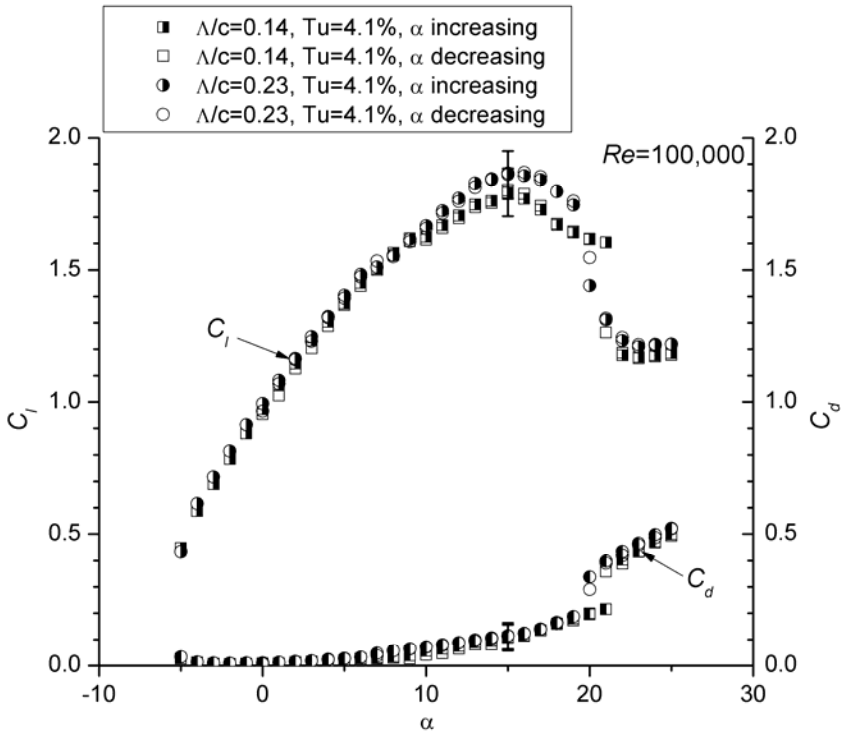

c)

Fig. 2.8 Comparison of coefficient of lift and drag at constant *Tu*=9.5%, with *Λ/c*=0.08 and *Λ/c*=0.14 mm. a) *Re*=55,000, b) *Re*=75,000, c) *Re*=100,000.

At *Tu*=9.5%, the integral length scale was increased from *Λ*=12 to 22 mm (*Λ/c*=0.08 to 0.14). At all Reynolds numbers tested (shown in Fig. 2.8), there is no significant difference in C_l and C_d between the two integral length scale cases. At *Re*=55,000 with *Λ/c*=0.08 (Fig. 2.8), the coefficient of lift continues to increase until it starts to decrease gradually at α=16 deg. The airfoil losses lift at α=17 deg for the case *Λ/c*=0.14. The coefficient of lift is generally higher with the larger integral length scale when α is between 16 and 25 deg. Similar phenomena are also shown at *Re*=75,000 (Fig. 2.8b) and *Re*=100,000 (Fig. 2.8c). An increase of $C_{l,max}$ is also seen with higher Reynolds numbers. No abrupt drop of lift is observed, and this is consistent with the high turbulence intensity case shown in Fig. 2.6.

However, It should be noted that with further increase in α after the airfoil reached $C_{l,max}$, the stall was delayed by 1 deg with the increase of the integral length scale, which contradicts the previous observation at *Tu*=4%; the airfoil stalled early with the larger integral length scale. We believe this contradiction may not exclusively be the result of the change in *Λ* but rather the result of different decaying rates of turbulence

intensity over the airfoil chord as previously mentioned. Although the turbulence intensity was maintained at 9.5% at the leading edge, the turbulence intensity, near the trailing edge, dropped to 6.5% for Λ/c=0.08 case, and 7.5% for Λ/c=0.14 case. The relative high turbulence intensity near the trailing edge, for the Λ/c=0.14 case, is believed to have more impact on the delay of the boundary layer separation as it enabled more momentum transfer between the outer flow and the boundary layer. It is difficult to generate Λ/c=0.23 at Tu=9.5%, but the differences are predicted to be small based on the current trend of airfoil performance with increasing length scale. Nevertheless, it is clear that the roles of integral length scale are subtle when the turbulence intensity is high.

Conclusions

The independent roles of turbulence intensity and turbulence integral length scale on the performance of an asymmetric, high-lift airfoil have been experimentally investigated at different Reynolds numbers. When the integral length scale was held constant, the stall of the airfoil was notably delayed for high angles of attack when the turbulence intensity was increased independently from Tu=4.1% to 9.5%. No abrupt loss of lift was observed at the high turbulence intensity. The lift decreased gradually after reaching peak value, indicating the separation point of the boundary layer transitioned from trailing edge towards the leading edge slowly.

The independent roles of the integral length scale were examined at two different turbulence intensity level Tu=4.1% and 9.5%. For the free-stream with low turbulence intensity (Tu=4%), the influence of the size of energy-containing eddies was prominent. The free-stream with small eddies (Λ/c=0.14, Λ=21 mm) delayed the stall of the airfoil at high angles of attack, indicating that the boundary layer did not separate suddenly from the airfoil. In contrast, the stall of the airfoil occurred at lower angles of attack with increasing a larger integral length scale (Λ/c=0.23, Λ=35 mm). It is believed that the boundary layer, formed under small energy-containing eddies, is less susceptible to the adverse gradient on the suction side of the airfoil. When turbulence intensity increased to Tu=9.5%, an increase in the integral length scale from Λ/c=0.08 to 0.14 did not change the lift and drag curve drastically. In the absence of the sudden drop of C_l beyond $C_{l,max}$, the effect of the integral length scale on the performance of the airfoil is found to be very small under higher turbulence intensity.

References

[1] Lissaman, P. B. S., "Low-Reynolds-Number Airfoils," Ann. Rev. Fluid Mech,1983, 15:223-39.

[2] Carmichael, B. H., "Low Reynolds Number Airfoil Survey," Vol. 1, 1981, NASA CR-165803.

[3] Mueller, T. J., and Batill, S. M., "Experimental Studies of Separation on a Two-Dimensional Airfoil at Low Reynolds Numbers," AIAA Journal, Vol. 20, No. 4, 1982, pp. 457-463

[4] Mueller, T. J., Prohlen, L. J., Conigliaro, P. E., and Jansen, B. J., "The Influence of Free-Stream Disturbances on Low Reynolds Number Airfoil Experiments," Experiments in Fluids, Vol. 1, 1983, pp. 3-14.

[5] Hoffmann, J. A., "Effects of Free-stream Turbulence on the Performance Characteristics of an Airfoil," AIAA Journal, Vol. 29, No. 9, 1991, pp. 1353-1354.

[6] Payne, F. M., and Nelson, R. C., "Aerodynamic Characteristics of and Airfoil in a Nonuniform Wind Profile," Journal of Aircraft, Vol. 22, No. 1, 1985, pp. 5-10.

[7] Devinant, Ph., Laverne, T., and Hureau, J., "Experimental study of wind-turbine airfoil aerodynamics in high turbulence," Journal of Wind Engineering and Industrial Aerodynamics, No. 90, 2002, pp. 689-707.

[8] Meier, H. U., and Kreplin, H. P., "Influence of Free-stream Turbulence on Boundary-Layer Development," AIAA Journal, Vol. 18, No. 1, 1980, pp. 11-15.

[9] Howard, R. H., and Kindelspire, D. W., "Free-stream Turbulence Effects on Airfoil Boundary-Layer Behavior at Low Reynolds Number," Journal of Aircraft, Vol. 27, No. 5, 1990, pp. 469-470.

[10] Sak, C., Liu, R., Ting, D. S-K., and Rankin, G. W., "The role of turbulence length scale and turbulence intensity on forced convection from a heated horizontal circular cylinder," Experimental Thermal and Fluid Science, Vol. 31, 2007, pp. 279-289.

[11] Selig, M. S., and Guglielmo, J. J., "High-Lift Low Reynolds Number Airfoil Design," Journal of Aircraft, Vol. 34, No. 1, 1997, pp. 72-79.

[12] Liu, R., Ting, D. S-K., and Checkel, M. D., "Constant Reynolds number turbulence downstream of an orificed perforated plate," Experimental Thermal and Fluid Science, No. 31, 2007, pp. 897-908.

[13] Liu, R., and Ting, D. S-K., "Turbulent Flow Downstream of a Perforated Plated: Sharp-Edged Orifice versus Finite-Thickness Holes," Journal of Fluids Engineering, Vol. 129, 2007, pp. 1164-1171.

[14] Coleman, H. W., and Steele, W. G., *Experimentation and Uncertainty Analysis for Engineers*, 2nd ed, John Wiley &Sons Inc., New York, 1999, p. 104.

[15] Selig, M.S., Guglielmo, J. J., Broeren, A.P., and Giguère, P., *Summary of Low-Speed Airfoil Data*, Vol. 1, SoarTech Publications, Virginia Beach, VA, 1995

CHAPTER 3. WAKE STRUCTURE UNDER THE INFLUENCE OF DIFFERENT TURBULENCE LEVEL

Introduction

The wake structure of an aerodynamic body has always been a major engineering research area since many fundamental characteristics of the flow around the subject, for example the behaviours of the boundary layer, can usually be revealed by investigating the wake [1]. In many engineering applications, wake survey assists engineers to study and estimate the aerodynamic performance of airfoils and turbine blades. Moreover, it also uncovers turbulence characteristics of the wake, which may significantly influence the performance of aerodynamic bodies operating downstream.

The performance of an airfoil in laminar free-stream is closely related to the behaviour of the boundary layer, and it has been well documented [2-5]. Lissaman has conducted an excellent review on the performance of airfoils [2]. The behaviour of the boundary layer is directly related to performance and the wake structure of airfoils. Campbell [6] examined turbulence intensity and power spectral density (PSD) behind a two-dimensional airfoil. Hah and Lakshminarayana [7] unveiled the complex nature of the near wake of a NACA 0012 airfoil by examining the mean velocity, turbulence intensity and Reynolds-stress across the wake. Huang and Lin [8] have found four characteristic modes of vortex shedding, which is closely related to the behaviour of the boundary layer instability on the suction side of the airfoil. At low angles of attack, the shear instability waves are stable only in the laminar shedding regime. The shear-layer instability frequency decreases with the increase in the angle of attack. At high angles of attack, the bluff-body effect dominates and no unique wave frequency is found. Yarusevych et al. [9] observed that the coherence and length scale of the wake vortices decrease significantly when the separation bubble forms on the upper surface of the airfoil. They conclude that the wake vortex shedding is attributed to the near-wake instability.

Free-stream turbulence has been known to have impacts on the performance of airfoils. Many researchers [10-15] conducted experiments with different free-stream turbulence intensities. In general, high turbulence level improves the lift coefficient and delays the stall of the airfoil to higher angles of attack due to its influence on the

boundary layer. For the wake structure, Huang and Lee [16] found that the free-stream turbulence has effects on the Strouhal number and Roshko number especially at low Reynolds numbers. Zhang et al, [17] examined the turbulence intensity effects on the wake structure of a pre-stall airfoil in a compressible, high speed environment. By increasing the turbulence intensity they found the velocity deficits become more uniform across the wake. The vortex shedding frequencies and strength are also observed to decrease with increasing turbulence level.

The turbulence integral length scale is another important parameter to describe turbulence, and it can usually be manipulated independently to the turbulence intensity. Some researchers have addressed its independent effects on aerodynamic bodies. For airfoils, Howard and Kindelspire [18] stated the importance of the length scale on the boundary layer of an airfoil: in order to affect the turbulent boundary-layer behaviour, the length scale must be on the order of the boundary-layer thickness. However, little literature addresses how the turbulence intensity and integral length scale independently affect the performance and the wake structure of an airfoil.

This study focuses on the independent effects of the turbulence intensity and integral length scale on the wake of an asymmetric, high-lift S1223 airfoil [19] at different Reynolds numbers. The wake of the airfoil is surveyed at different turbulence levels. The mean velocity and turbulence intensity profile together with PSD are examined systematically at the stall and post-stall region.

Experimental Methods

Wind Tunnel

The experiment was carried out in a closed-loop wind tunnel with the test section to be nominally 4 m long, 0.762 m high by 0.762 m wide. The velocity of the wind tunnel can be adjusted between 3 and 20 m/s with the test section empty. The turbulence level of the incoming flow is around 0.5%.

Airfoil

A S1223 high-lift asymmetric airfoil was used in the experiment. The airfoil was carved out of a piece of maple wood on a numerically controlled milling machine. A thin layer of Bondo® glazing and spot putty was applied on the surface to fill the wood pore.

The model was sanded by grit 1500 sand paper before it was painted in white. Finally, clear acrylic paint was applied and buffered by using NOVUS plastic polish No.2 to improve its smoothness. The chord of the airfoil is 0.1524 m (6 in) with span-to-chord ratio of 5.0.

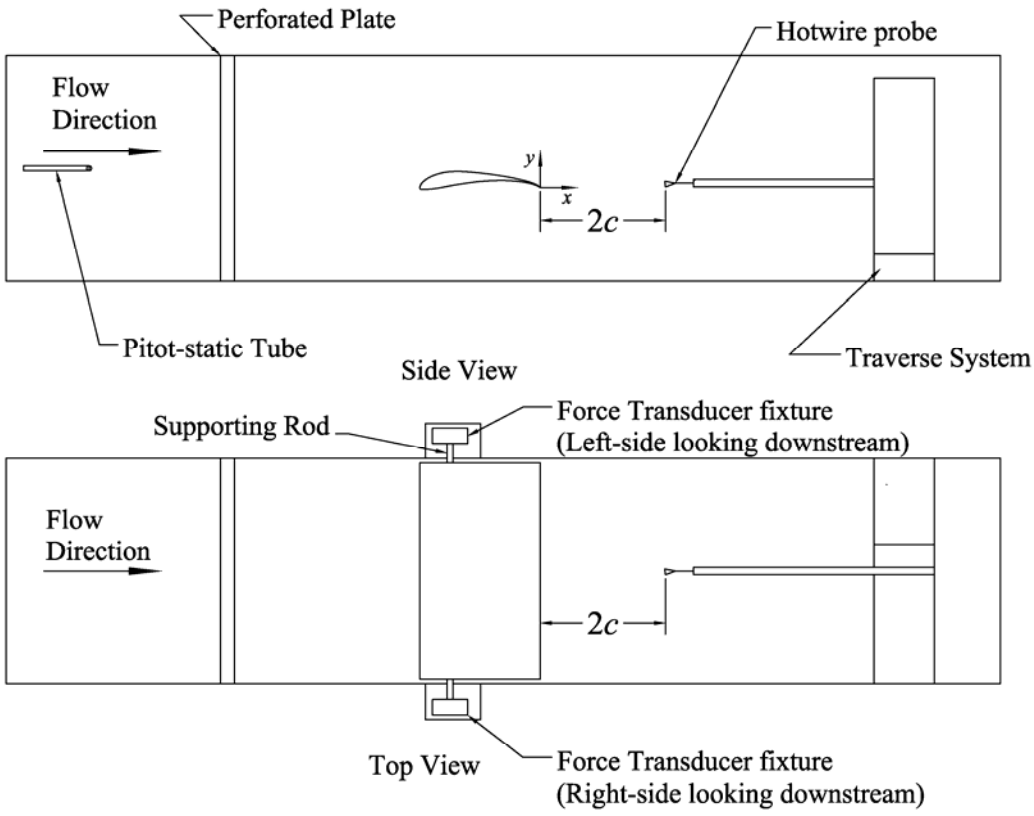

Fig. 3.1 Wind tunnel configuration of the experimental setup.

Force Measurement

The airfoil model was mounted horizontally 0.394 m above the wind tunnel floor and 3.33 m downstream of the inlet of the test section (Fig. 3.1). It spans across the tunnel test section. The gap between the end of the model and the tunnel wall was maintained nominally at 0.1 in at each side. At a quarter chord length from the leading edge, a supporting rod was inserted to each end of the airfoil and secured by a set screw. The other end of the supporting rod was connected to the bearing mounted on the force transducer fixture so that the airfoil could freely rotate. To restrain the rotation of the airfoil, two set screw knobs were added to the left-side fixtures to fix the desired angle of

attack (Fig. 2.4). A protractor was added, and it could rotate with the airfoil to indicate the angle of attack with accuracy of +/-0.3 deg.

Two ATI Gamma type six-component strain force/torque transducers were utilized in this experiment. On the right-side looking downstream (Fig. 3.1), a transducer with maximum force measuring range +/-65N was mounted on an aluminium structure attached to the wind tunnel. With the similar setup on the other side, the maximum range of the force transducer was +/-32N. The transducers were carefully positioned and calibrated using weight before the experiment so that the positive *y*-axis of the transducer pointed up perpendicular to the flow for the lift measurement, and the *x*-axis was aligned with the direction of flow. The uncertainty of the angle between the *y*-axis of transducer and vertical direction was less than 0.3 deg. The summation of the force components in *y*-direction was lift, and the summation of the force components in *x*-direction was drag. At each angle of attack, 20,000 force samples were recorded during a 20 sec period. The sampling rate was 1 kHz. The overall uncertainty lift and drag coefficient was estimated to be less than 5%.

Turbulence Generator

Turbulence was generated by orificed perforated plates [20, 21]. The plates were manufactured by drilling a matrix of chamfered orificed holes on a 3 mm-thick aluminium sheet. The sharp-edged design not only reduces the thickness effect of the plate on the turbulence structure but also provides a better quasi-isotropic turbulent flow compared to conventional solid-bar turbulence generation grids [21]. Without the presence of the airfoil, the free-stream turbulence was evaluated with a hot-wire anemometer placed at the center of the cross plane where the leading edge of the airfoil were to be located. The turbulence parameters and their uncertainties are listed in Table 2.1.

Wake Measurement

Wake survey was conducted using a Dantec streamline 55C90 constant temperature anemometer with a Dantec Type 55P01 single-wire gold-plated probe. The probe was placed x/c=2 behind the trailing edge of the airfoil (Fig. 3.1) and traversed in the vertical mid-span plane. The analog voltage signal was first low-passed at 30 kHz

using an analog filter to avoid aliasing. Then it was sampled at 80 kHz over 25 s period through a 12 bit PCI-6071E National Instrument data acquisition card. The distance between each point across the wake is 6.35 mm (0.25 in). Power spectral density was estimated in MATLAB using Welch's method [22]. By using this method, the stream-wise velocity fluctuation component was sectioned into a series of segments, each containing 2^{16} samples with 50% overlap. A 2^{18} length of fast Fourier transform was performed on each segment, and the final PSD was ensemble-averaged. The resolution of the spectrum is 0.305 Hz.

Results and Discussion

The wake structures at stall and post-stall angles of attack are discussed in detail because prominent differences are observed.

Turbulence intensity effects

The turbulence intensity effects on the lift coefficients are first compared in Fig. 3.2 at Re=55,000 and Re=100,000 specifically. Without installing any perforated plate (Tu<0.5%) at Re=55,000 (Fig. 3.2a), the maximum lift coefficient occurs at α= 4 deg, and a sharp drop of C_l is at α= 5 deg indicating that the airfoil stalls. After the free-stream turbulence intensity increases to 4.1% with Λ/c=0.14, the slope of the lift coefficient shows a slight decrease between α=-5 to 4 deg. However, the maximum lift coefficient is greatly improved to reach 1.81 at α=16 deg. Although the lift coefficient decreases slightly with the further increase in the angle of attack, the stall does not occur until α=19 deg. At Tu=9.5% with Λ/c=0.14, the lift coefficient curve behaves the same as the one at Tu=4.1%. Pronounced differences can be seen beyond α=18 deg, where the lift coefficient at highest Tu decreases gradually when increasing the angle of attack, and no sharp drop of C_l is observed comparing to previous cases.

The free-stream turbulence intensity has the same effects at Re=100,000 (Fig. 3.2b). In general, the slope of the lift coefficient decreases with increasing the free-stream turbulence intensity. When the free-stream turbulence intensity level is raised from Tu=0.5% to Tu=4.1%, an increase in maximum lift coefficient at α=15 deg and a delayed stall at α=22 deg is clearly shown. These phenomena generally agree with the

observation by Hoffman [11], Payne and Nelson [12] for other airfoils. By further increasing the free-stream turbulence to Tu=9.5%, the lift is slightly lower below α=15 deg. On the other hand, the lift coefficient, for Tu=9.5%, is consistently higher beyond α=22 deg comparing to the Tu=4.1%. The doubled turbulence intensity at high turbulence level does not improve C_l before reaching its peak value; however, the fundamental influence of the turbulence level is to delay or eliminate the sharp loss of lift by delaying the boundary layer separation near the trailing edge, and this could be supported by the examination of the wake structure.

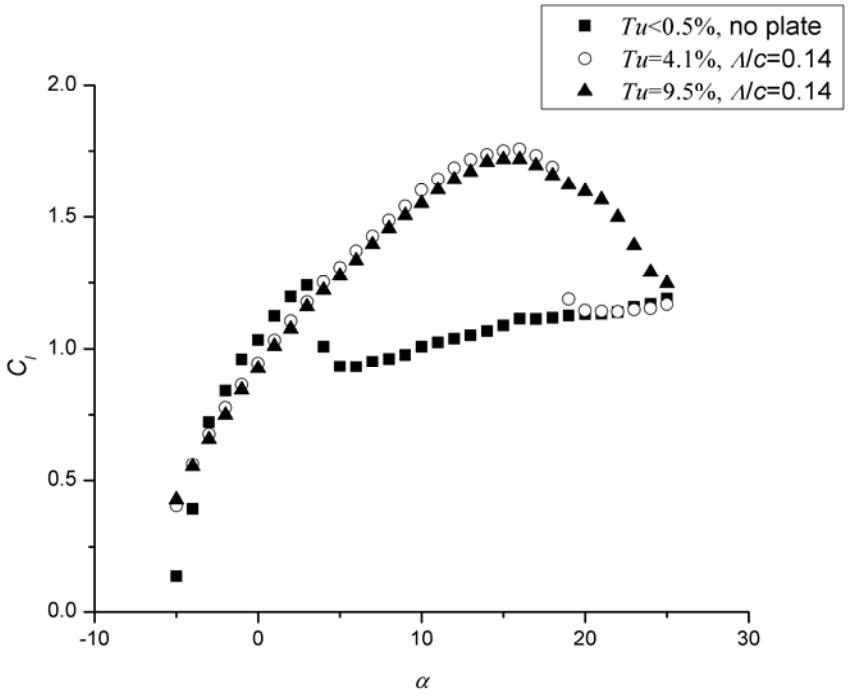

a)

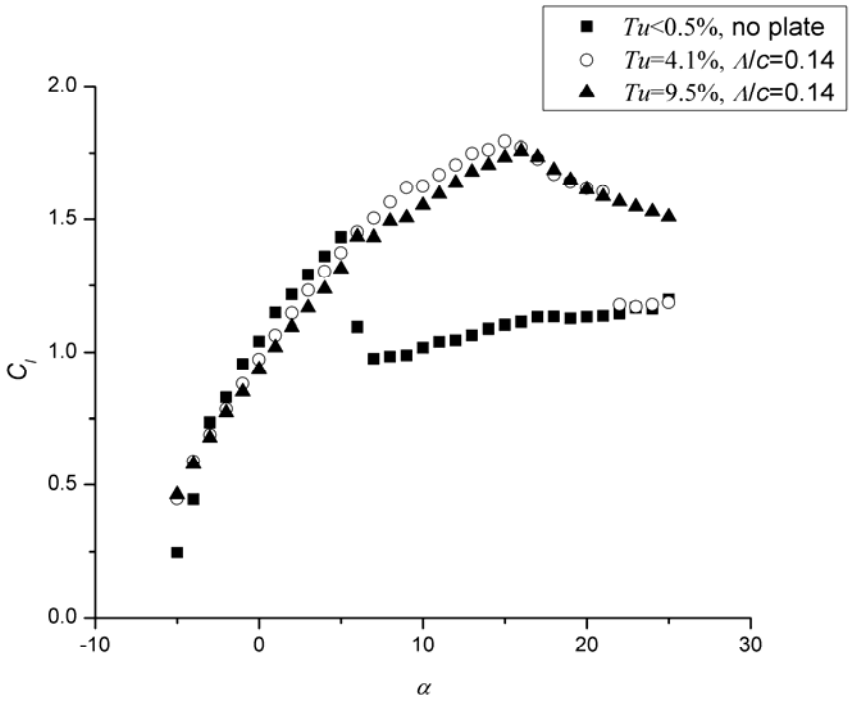

b)

Fig. 3.2 Comparison of lift coefficients under different free-stream turbulence intensities. a) *Re*=55,000, b) *Re*=100,000.

The normalized mean-velocity deficit profiles and turbulence intensity profiles are plotted in Fig. 3.3 as the free-stream turbulence intensity was increased independently from Tu=4.1% to 9.5% with constant integral length scale Λ/c=0.14 (Λ=21 mm). Also the profiles without any perforated plate (Tu<0.5%) are plotted to assist analysis. The wakes are investigated in detail at angles of attack α= 20 deg for Re=55,000 and α= 23 deg for Re=75,000 and 100,000. It was found by preliminary testing that the airfoil stalled at theses angles of attack. At Re=55,000, the wake generated without any perforated plate is the widest and have the largest velocity deficits. At Tu=4.1%, a narrower wake was formed behind the airfoil with the maximum velocity deficit to be 0.37 (Fig. 3.3a). When the free-stream turbulence intensity increases to 9.5%, the wake becomes even narrower, and the maximum velocity deficit reduces to 0.28. It has also been observed that drastic decrease of the velocity deficit occurred at the upper and the middle part of the wake with increasing the free-stream turbulence intensity (Tu=4.1% to 9.5%). However, the velocity deficit remains relatively unchanged at the lower part of the wake. As a result, the velocity profile skews downwards to the negative direction of the y-axis. These general effects of the turbulence intensity in weakening, narrowing, and skewing of the wake are consistent at higher Reynolds numbers. At Re =75,000 shown in Fig. 3.3b, the maximum velocity deficit is 0.43. Increasing the free-stream turbulence intensity reduces it to 0.32. The position of the maximum velocity moves from y/c= -0.125 to 0.25. At Re =100,000 (Fig. 3.3c), the maximum velocity deficit decreases from 0.43 to 0.32 as well, and its corresponding position reduces from y/c=-0.125 to 0.25.

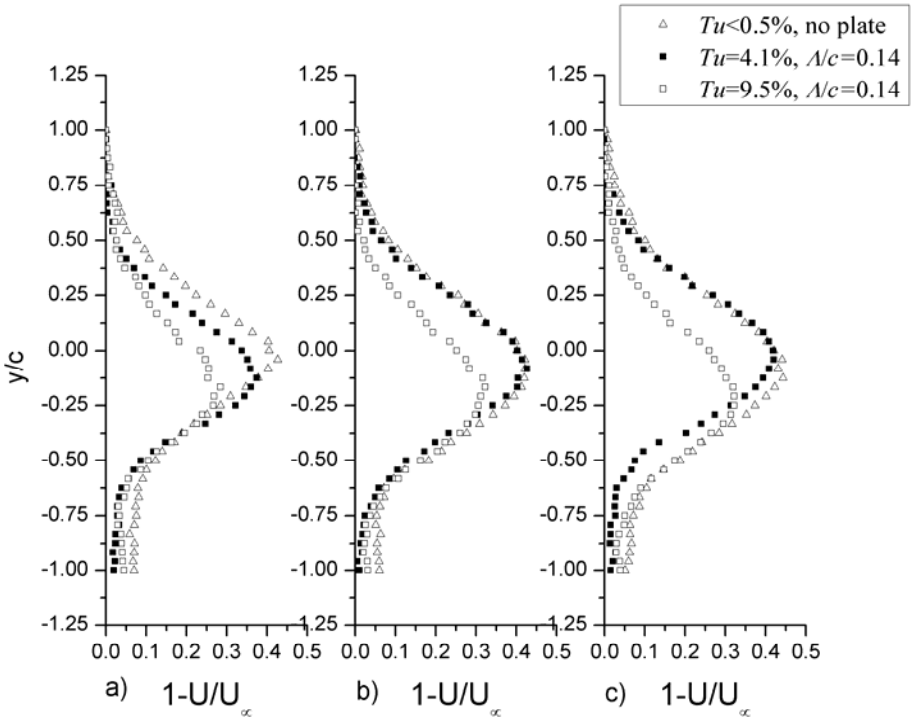

Fig. 3.3 Comparison of velocity deficits at around Λ/c=0.14, with *Tu*=4.1% and 9.5%. a) *Re*=55,000, α=20 deg, b) *Re*=75,000, α=23 deg, c) *Re*=100,000, α=23 deg.

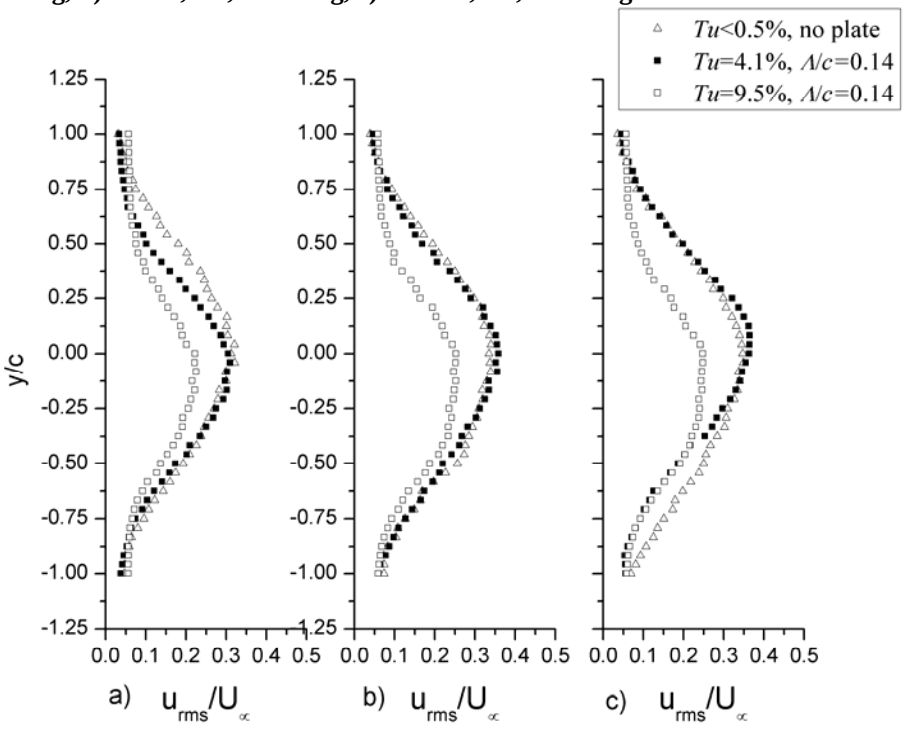

Fig. 3.4 Comparison of turbulence intensity at around Λ/c=0.14, with *Tu*=4.1% and 9.5%. a) *Re*=55,000, α=20 deg, b) *Re*=75,000, α=23 deg, c) *Re*=100,000, α=23 deg.

The turbulence intensity profiles (Fig. 3.4) also share similar trends as the velocity deficit profiles. At Re=55,000, the wake turbulence intensity is the highest at the upper part of the wake (Tu<0.5%). A remarkable decrease in the wake turbulence is observed as the free-stream turbulence intensity increases from 4.1% to 9.5%. For all Reynolds numbers examined at high level turbulence intensity, a suppression of the wake turbulence intensity is clearly seen on the upper and center part of the wake when the free-stream turbulence level is higher, whereas the change is subtle at the lower part of the wakes under different free-stream turbulence conditions. A large flat region with little variation in turbulence intensity is also shown in the middle part of the wake (from y/c=-0.3 to y/c=0), and it becomes prominent especially at Re=75,000 (Fig. 3.4b) and 100,000 (Fig. 3.4c). The reduced turbulence intensity level indicates the boundary layer is likely still attached to the airfoil with little separation. In general, the wake is widest when Tu<0.5%. With elevated free-stream turbulence intensity, the wake narrows.

The corresponding lift and drag measurements support the observation of the wake (Table 3.1). The lift and drag coefficients are identical between Tu<0.5% and Tu=4.1% cases. However, high free-stream turbulence intensity results an increase in C_l and a decrease in C_d. For Re =55,000 at Tu=4.1%, the lift coefficient and drag coefficient are calculated to be 1.19 and 0.39, and this corresponds to a high velocity deficit and wide wake. When the turbulence intensity is increased to 9.5%, the lift coefficient increases to 1.59 and the drag coefficient reduces to 0.21, and a shallow velocity deficit profile and a narrower wake are observed. At Re =75,000 and Re =100,000, a 28% increase of lift and 42% decrease of drag are also prominent when free-stream turbulence level is higher. It can be understood that high free-stream turbulence intensity helps to generate more lift and reduce drag by suppressing the boundary layer separation. Without the separation, the velocity deficit and the turbulence intensity in the wake become small.

Table 3.1 Turbulence intensity effect

	Free-stream condition	C_l	C_d
Re=55000,	*Tu*<0.5%, no plate	1.14	0.37
α= 20 deg	*Tu*=4.1%, Λ/c=0.14	1.19	0.39
	Tu=9.5%, Λ/c=0.14	1.59	0.21
Re=75000,	*Tu*<0.5%, no plate	1.18	0.43
α= 23 deg	*Tu*=4.1%, Λ/c=0.14	1.23	0.49
	Tu=9.5%, Λ/c=0.14	1.57	0.28
Re=100,000,	*Tu*<0.5%, no plate	1.22	0.47
α= 23 deg	*Tu*=4.1%, Λ/c=0.14	1.24	0.49
	Tu=9.5%, Λ/c=0.14	1.55	0.29

The power spectral density of the longitudinal velocity component is plotted at multiple vertical locations across the wake. Two orders of magnitude offset are used for the amplitude for clarity, and the vertical scale is arbitrary for all PSD.

When free-stream turbulence intensity *Tu*<0.5%, vortex-shedding frequency is seen at *f*=16 Hz (Fig. 3.5a). Strong peaks centered at this frequency are shown across the wake, and the amplitude only decreases approach the center of the wake (*y/c*=0). The harmonic frequencies are also identified at *f*=32 Hz and higher frequencies.

Frequency components are detectable at *Tu* =4.1% centered at *f*=17 Hz for *Re*= 55,000 (Fig. 3.5b). Although the amplitude is reduced and contaminated with noise, the peak is unambiguous at the upper part of the wake. As the location approaches to the center of the wake, the strength of the peak diminishes. No peak is observable around the center of the wake located at *y/c*=-0.25. Approaching to the lower part of the wake, the same frequency content reappears and is strengthened (e.g. *y/c*=-0.25 to -1). At higher Reynolds numbers, peaks centered at *f*=20 Hz for *Re*=75,000 and *f*=25 Hz for *Re*=100,000 are observed. The PSD across the wake suggests two separate rows of vortices were formed at the upper and lower part of the wake as a result of the boundary layer separation. The airfoil thus behaves like a bluff-body, and the separated upper and lower shear layers develop independently as they are far spaced apart and failed to interact with each other. The upper row of the vortices may be formed due to the

instability of the separated boundary layer on the suction side, and the lower row may form at the trailing edge of the airfoil.

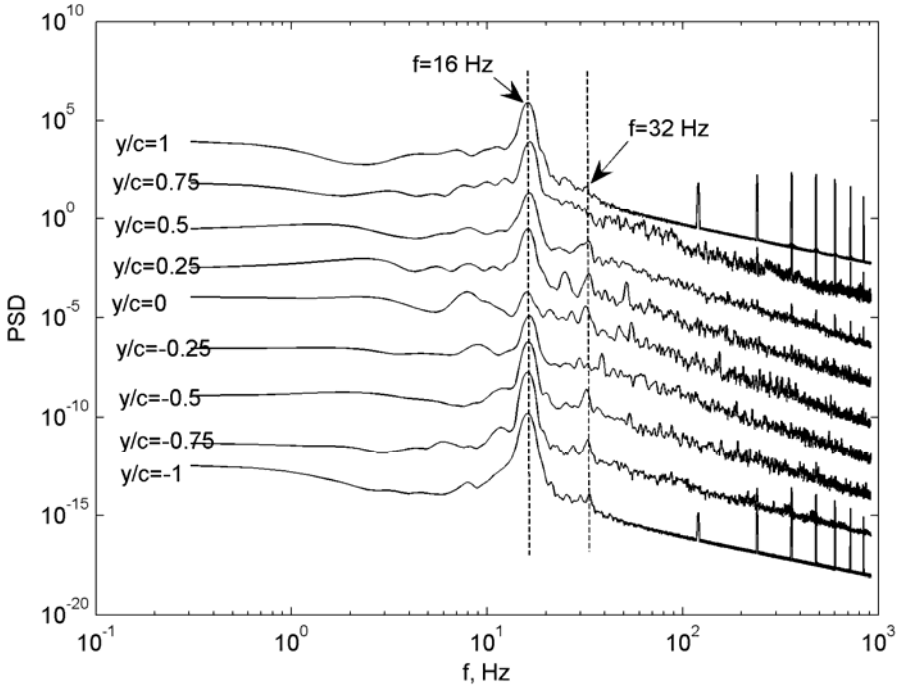

a)

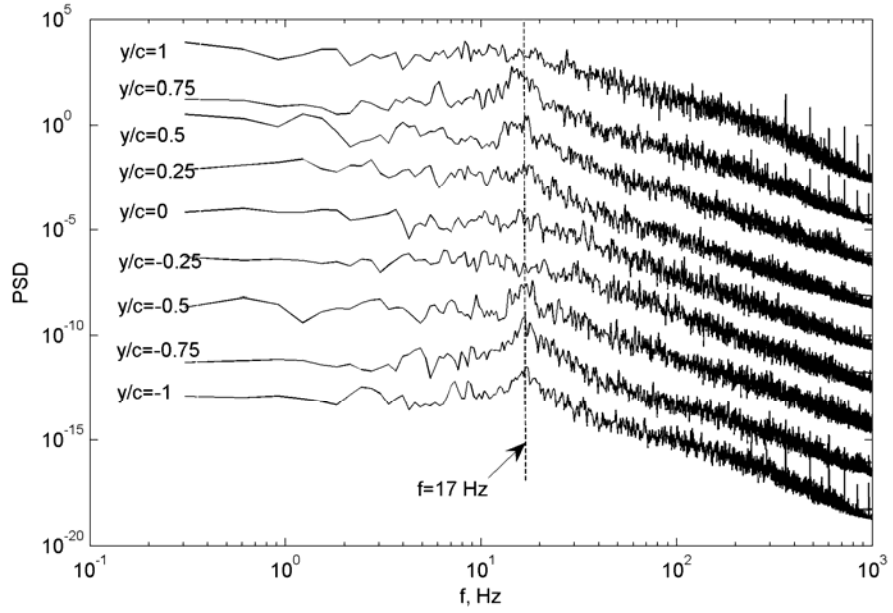

b)

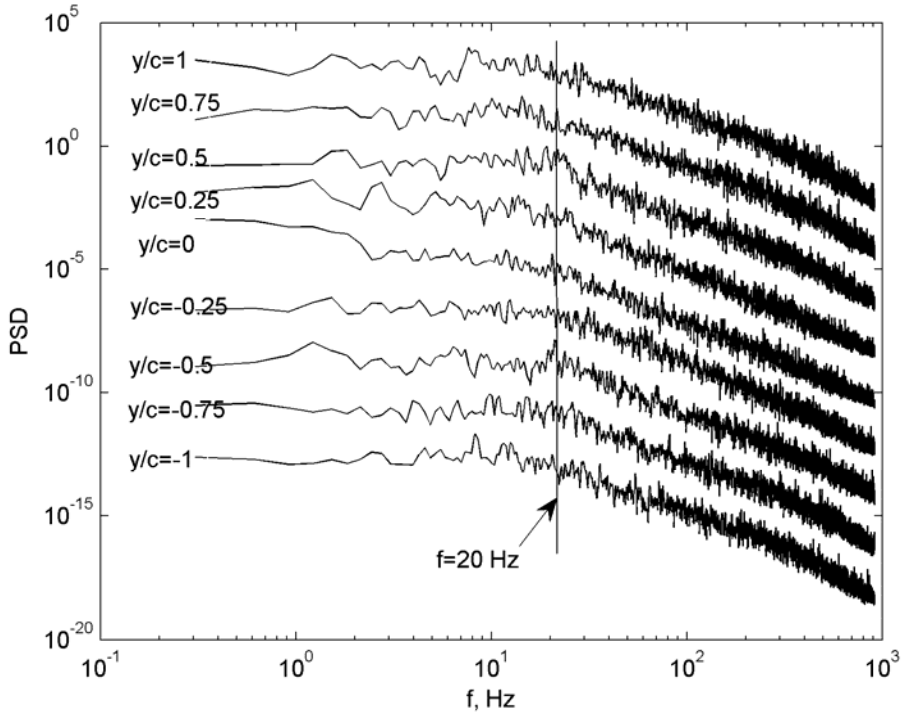

c)

Fig. 3.5 Comparison of PSD at different vertical locations across the wake with *Re*=55000, b) *Tu*<0.5%, no plate, b) *Tu*=4.1%, *Λ/c*=0.14, c) *Tu*=9.5% *Λ/c*=0.14.

When the free-stream turbulence intensity is increased to *Tu*=9.5%, the magnitude of the peak is much less observable, detectable peaks only appears at lower part of the wake. It indicates the strength of the vortices weakened due to the strong interaction between outer-flow and the boundary layer. Vortex shedding frequency has a marginal increase to 20 Hz at *Re*=55,000 (Fig. 3.5c), 25 Hz for *Re*=75,000, and 32 Hz for *Re*=100,000.

Obviously, the strong frequency-centred feature at low turbulence intensity indicates vortex-shedding as a result of the boundary layer separation. As the separation initiates, the wake widens, and the velocity gradient in the wake grows accordingly. Large vortices, containing more momentum, form due to the instability at the boundary layer separation point on the lifting-surface and at the trailing edge. This causes prominent peaks in PSD. As the turbulence intensity increases, more momentum is exchanged between the outer-flow and the boundary layer, which enables the boundary layer to remain attached to the suction side. And the vortex shedding phenomenon is less observable.

In general, the independent effect of the free-stream turbulence intensity is significant in delaying the stall. Low free-stream turbulence intensity appears to have less energy infused to the boundary-layer. This leads to the early separation of the boundary layer and results a large wake. In contrast, high free-stream turbulence intensity, by carrying more energy with it, helps the momentum exchange between the outer-flow and the boundary layer. With momentum influx from the free-stream, the high inertia boundary layer becomes less susceptible to the large adverse pressure gradient on the upper side of the airfoil at high angles of attack. Consequently, the boundary layer is much suppressed, and the wake is much narrower when increasing the free-stream turbulence intensity.

Integral length scale effects

The independent effects of integral length scale are examined at two different turbulence intensities Tu=4.1% and 9.5%. For Tu=4.1%, the integral length scale is increased from Λ/c= 0.14 to 0.23 (Λ= 21 to 35 mm). The velocity deficit profiles and turbulence intensity profiles are compared at stall and post-stall angles of attack α=18 and 20 deg for Re=55,000 (Fig. 3.6a and b), α=20 and 23 deg for Re=75,000 (Fig. 3.6c and d), and α= 21 and 23 deg for Re= 100,000 (Fig. 3.6e and f). For Re=55,000 at α= 18 deg, large velocity deficits are clearly seen on Fig. 3.6a. With increasing the integral length scale, the maximum velocity deficit increase from 0.21 to 0.43 and the wake is widened. At α=20 deg (Fig. 3.6b), the wake becomes wider for both cases with the maximum velocity deficits increasing from 0.25 to 0.4.

At higher Reynolds numbers and angles of attack, the differences in the velocity deficit at stall angles of attack become more prominent. The velocity profiles have little difference at the upper part of the wake for Re=75,000 at α= 20 (Fig. 3.6c) and Re=100,000 at α= 21 deg (Fig. 3.6e). The effects of the turbulence length scale are seen at the center and lower part of the wake profile. Increasing the length scale from Λ/c=0.14 to 0.23 makes the profiles reach high velocity deficits. It also widens and skews the profiles to the negative direction of y-axis. At the incidence angle α= 23 deg, widened wakes are seen in Fig. 3.6d and f. The differences of the deficit profiles under different free-stream length scales are small compared to ones at α= 21 deg (Fig. 3.6c and e). It

indicates the influence of Λ/c becomes subtle with increasing the angle of attack passing the stall region.

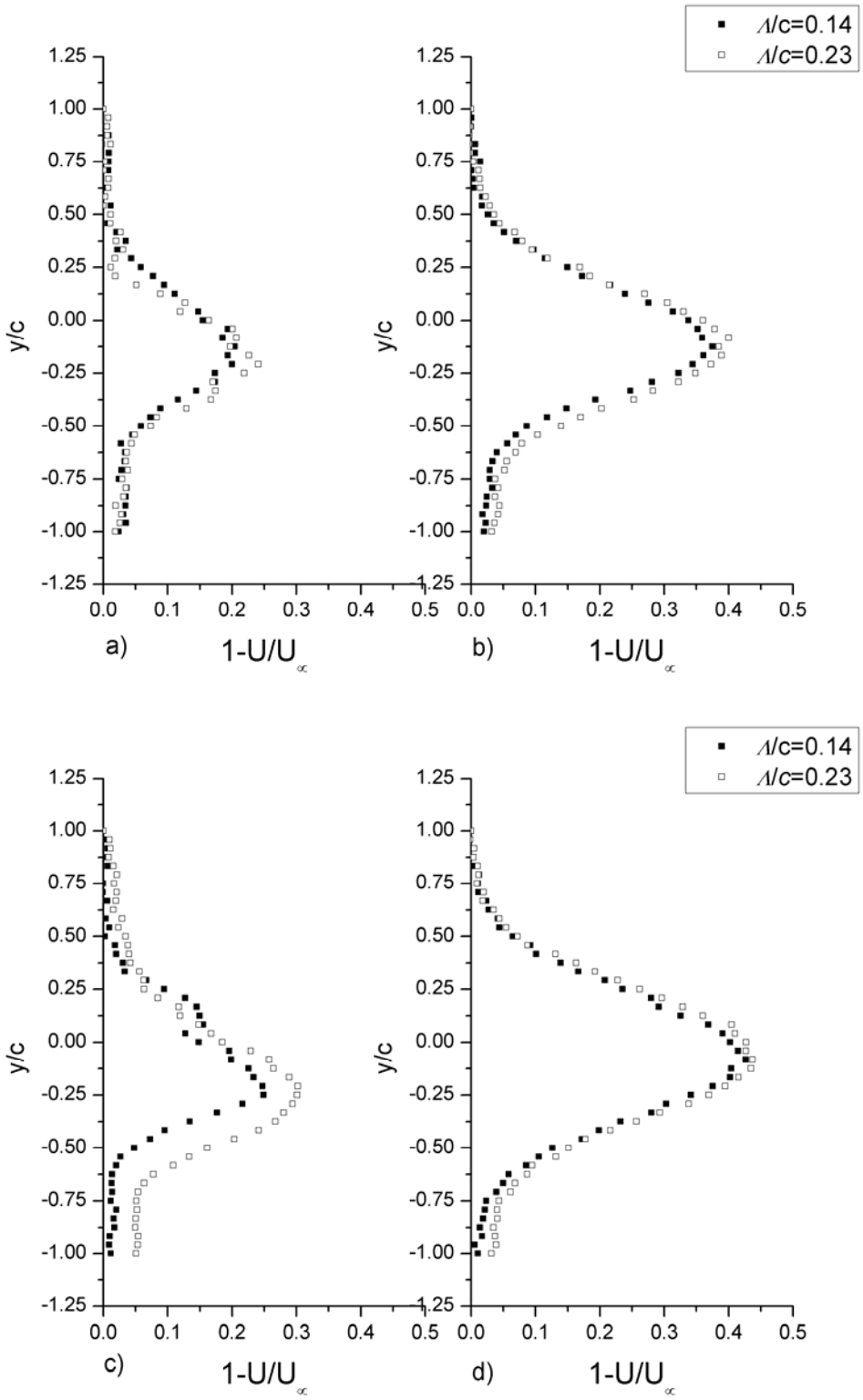

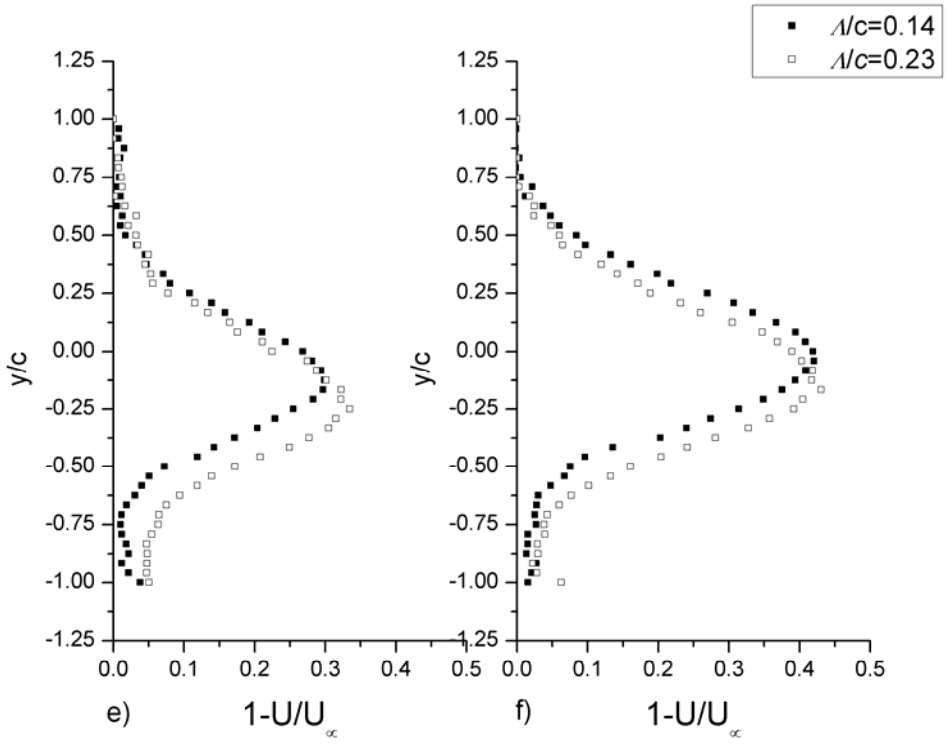

Fig. 3.6 Comparison of velocity deficits at constant *Tu*=4.1%, with *Λ/c*=0.014 and *Λ*=0.023: a) *α*=18 deg and b) *α*=20 deg for *Re*=55,000, c) *α*=20 deg and d) *α*=23 deg for *Re*=75,000, e) *α*=21 deg and f) *α*=23 for *Re*=100,000.

Fig. 3.7 shows the wake turbulence intensity level with increasing free-stream length scale from *Λ/c*= 0.14 to 0.23. Fig. 3.7a illustrates the wake turbulence level at *Re*=55,000 and *α*= 18 deg. At *Λ/c*= 0.14, a bell shaped turbulence level profile is seen with the maximum value located at *y/c*=0.0625. At *Λ/c*= 0.23, the turbulence level remains constant at 0.04 from *y/c*=1 to 0.25. Moving downwards, there exists an abrupt increase of the turbulence level to 0.25. Large fluctuations of turbulence level across the wake is observed especially between *y/c*=-0.25 and -0.5. It has been observed the lift coefficient was not stable during the wake survey at *Re*=55,000 at the stall angle of attack. Together with the observation on the unstable turbulence intensity across the wake it indicates the boundary layer behaviour is very sensitive turbulence at low *Re*=55,000. Besides the increased wake turbulence intensity with high *Λ/c*, the wake profile also shifts downwards. When the angle of attack increases to *α*= 20 deg, the wake for both cases becomes wider with maximum turbulence level at the wake centre (*y/c*=-0.125). The shape of the wake profiles is identical. The profiles at *Re*=75,000 have similar trend

as observed at *Re*=55000: at α= 20 (Fig. 3.7c) deg, the wakes profiles show irregularities for both cases, and the profile skew downwards with higher the Λ/c; at α= 23 (Fig. 3.7d), the location of the maximum turbulence level shifts upwards to *y/c*=0, while the difference of the wake profiles between two cases is nearly undetectable. The irregular wake profile shape persists when *Re*=100,000 at α= 21 deg. Increase the angle of attack to 23 deg, the wake is widened. However, a downward skew of the profile under high integral length scale Λ/c = 0.23 is observed, and this phenomenon is not shown at *Re* = 55000 (Fig. 3.7b) and *Re* = 75,000 (Fig. 3.7d). It is a question whether the higher Reynolds number plays a role, or it is simply due to the uncertainty of the angle of attack; that is, α at high Λ/c is lower thus shifts the wake downwards.

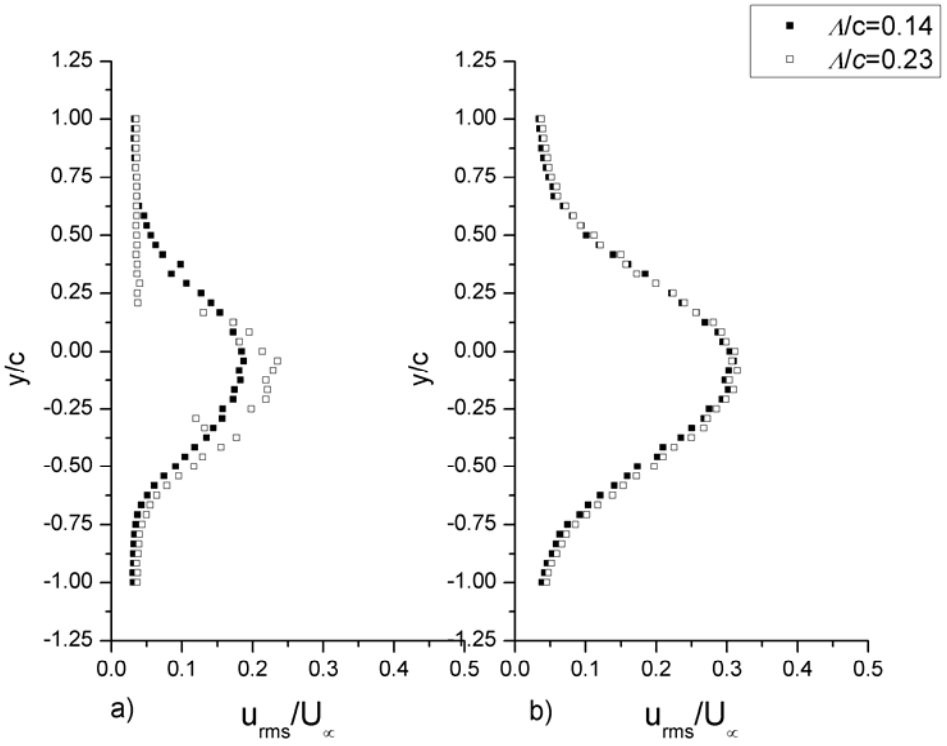

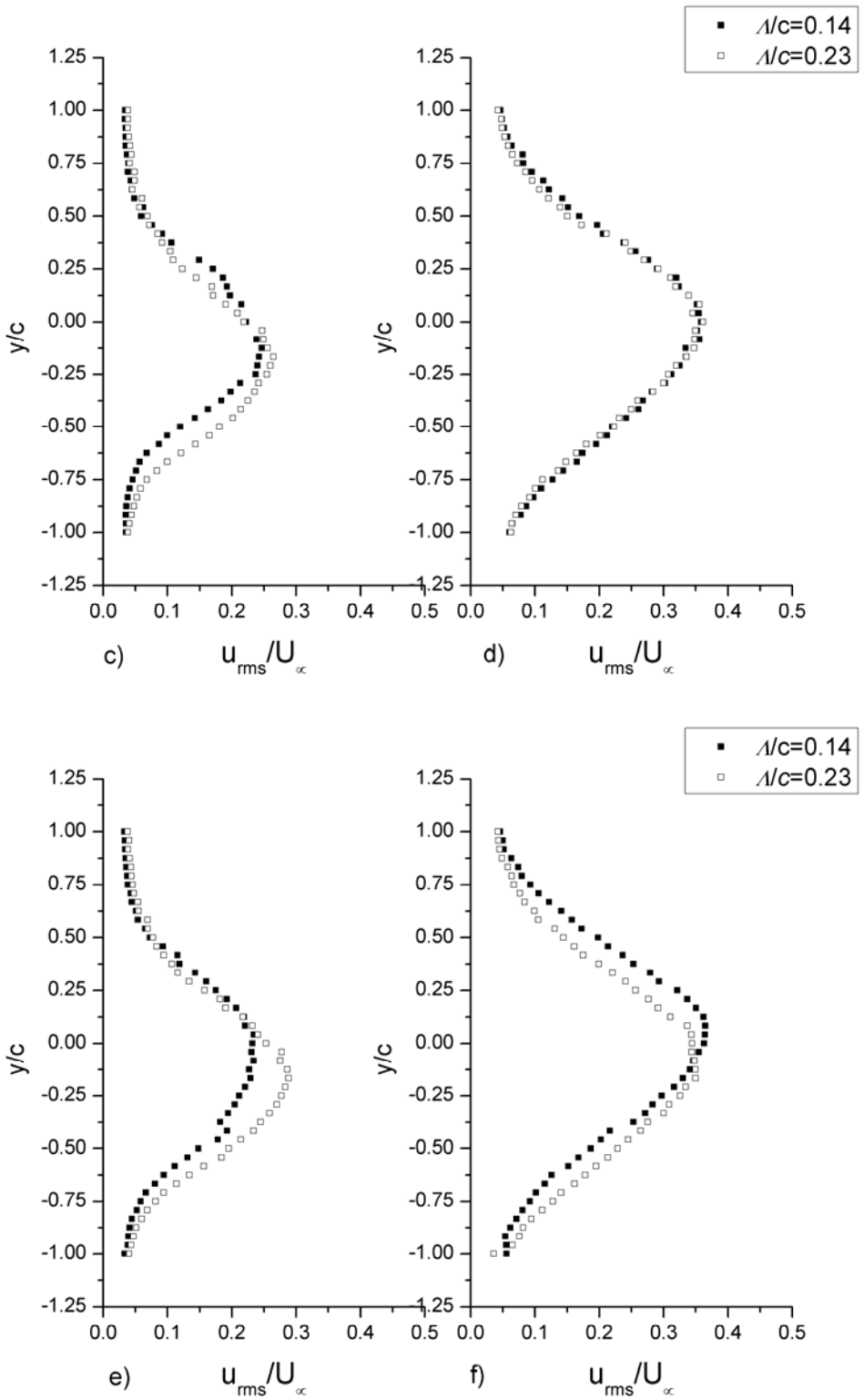

Fig. 3.7 Comparison of turbulence intensity profiles at constant *Tu*=4.1%, with *Λ/c*=0.014 and *Λ*=0.023: a) *α*=18 deg and b) *α*=20 deg for *Re*=55,000, c) *α*=20 deg and d) *α*=23 deg for *Re*=75,000, e) *α*=21 deg and f) *α*=23 for *Re*=100,000.

Generally speaking, the irregularities presented in Fig. 3.7a, c, and e, for all Reynolds number reveal the wake structure of the airfoil is unstable under the influence of the turbulence at the stall angle of attack. This is the direct result of the unstable boundary layer, and it indicates that the wake structure at these angles of attack is modified constantly by the free-stream turbulence integral length scale. As the angle of attack increases, the wake structure becomes more stable, and the role of the length scale becomes subtle.

Table 3.2 lists the lift and drag data at all Reynolds numbers. At the same angle of attack and Reynolds number, the lift coefficient of the airfoil decreases under the large free-stream integral length scale (Λ/c=0.23), and the drag coefficient shows an increase. It supports the observation on the wake survey. A wider wake indicates the initiation of the boundary layer separation from the upper surface of the airfoil, and it triggers the degradation of the performance of the airfoil. Differences in C_l and C_d at the post-stall angles of attack are subtle.

Table 3.2 Independent effect of turbulence integral length scale at *Tu*=4.1%

	Free-stream condition	C_l	C_d
Re=55000, α= 18 deg	Λ/c=0.014	1.74	0.14
	Λ/c=0.023	1.29	0.34
Re=75000, α= 20 deg	Λ/c=0.014	1.64	0.21
	Λ/c=0.023	1.32	0.38
Re=100,000, α= 21 deg	Λ/c=0.014	1.62	0.24
	Λ/c=0.023	1.31	0.42

The PSD is plotted at y/c=-0.5 with different free-stream integral length scale in Fig. 3.8. At *Re*= 55,000 and α= 18 deg (Fig. 3.8a), a peak centered at around f=25 Hz can be spotted. It reveals that frequency-centered activity is presented in the wake. With the increasing angle of attack to α=20 deg, a relatively broad and strengthened peak is evident at a frequency around f=16 Hz for both cases (Fig. 3.8b). This is due to large low frequency vortex structures generated in the wake. And the decrease of vortex-shedding frequency indicates an increase in the length scale of the vortices. At *Re*=75,000, a small peak centered at f=24 Hz is detected only with free-stream Λ/c=0.23 (Fig. 3.8c). Further

increasing the angle of attack to 23 deg, a sharp peak appears again for both cases at f=20 Hz (Fig. 3.8d). A very subtle peak at f =24 Hz is seen at Λ/c=0.23 for the highest Reynolds number (Fig. 3.8e). Whereas sharper peaks appear at post-stall region (Fig. 3.8f) with f=26 Hz respectively for both cases. At post-stall angles of attack, vortex-shedding frequency increases as the Reynolds number increases. However, the strength of the frequency-centered activities decreases at Re=100,000 with Λ/c=0.23. It may indicate the change of the wake structure (or the location of the vortices) and the length scale of the vortices under the influence of the free-stream integral length scale. Different integral length scales influence the wake structure and the performance of the airfoil significantly at stall angles of attack; however, the wake structure at post-stall angles of attack does not greatly altered by the current level free-stream length scale.

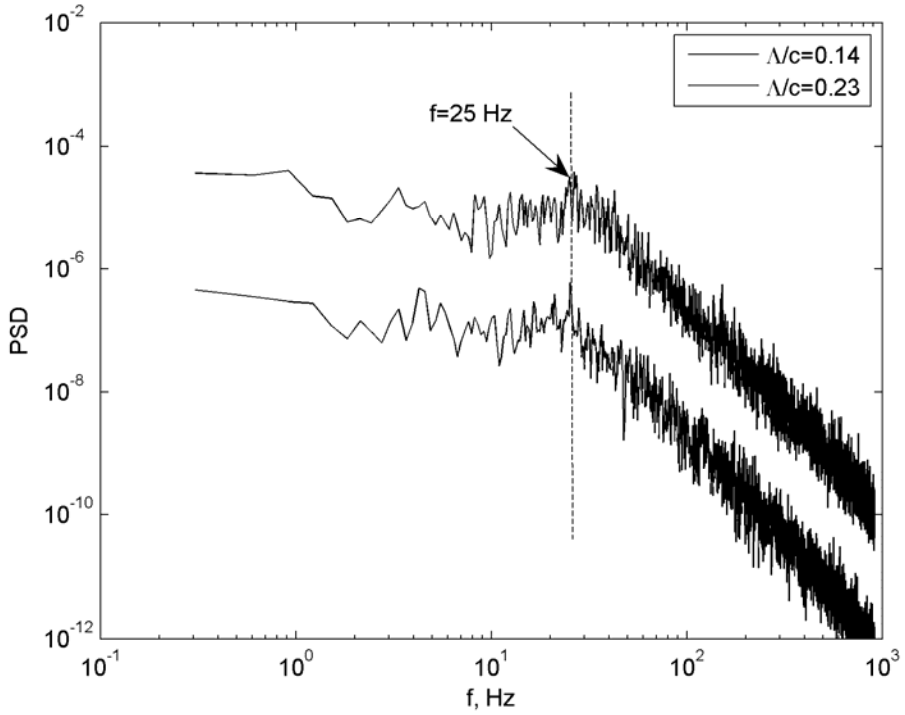

a)

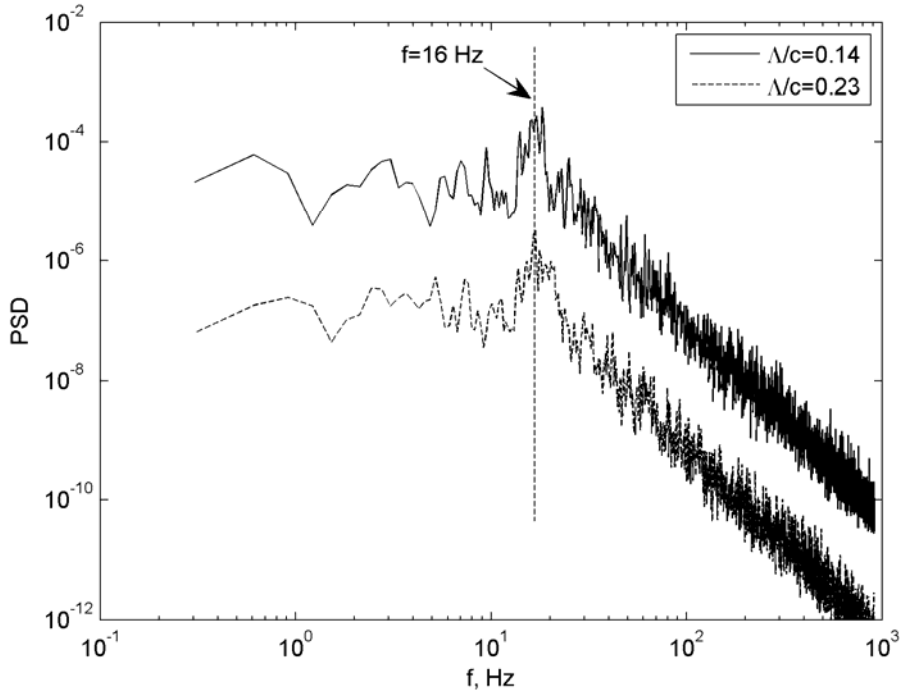

b)

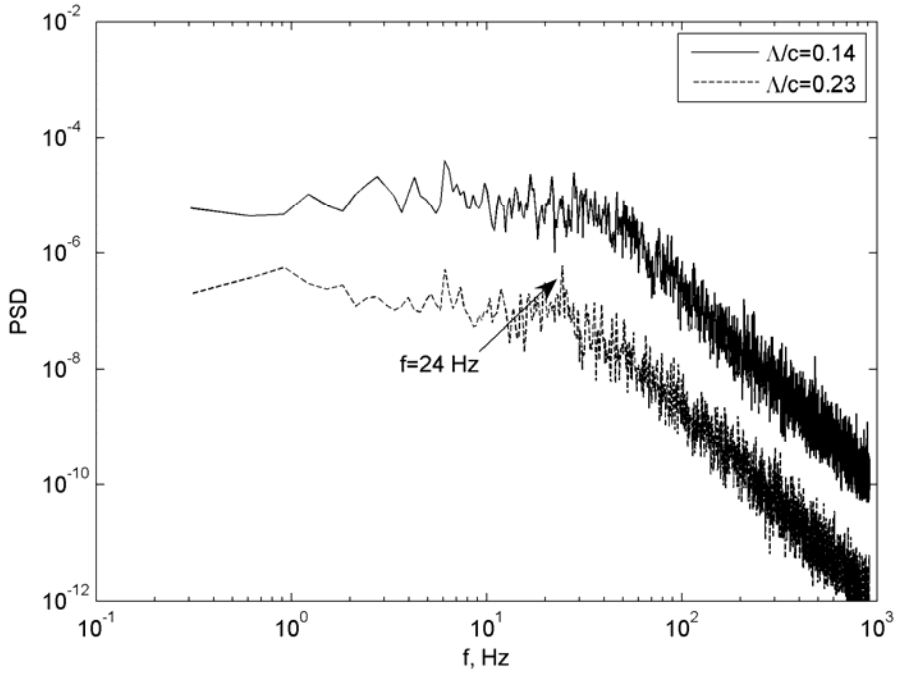

c)

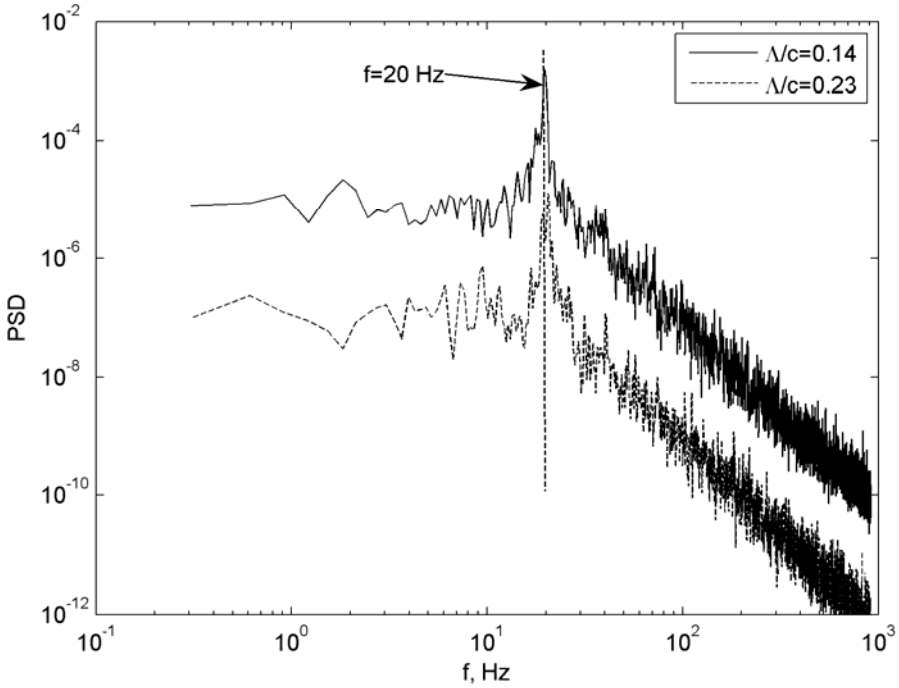

d)

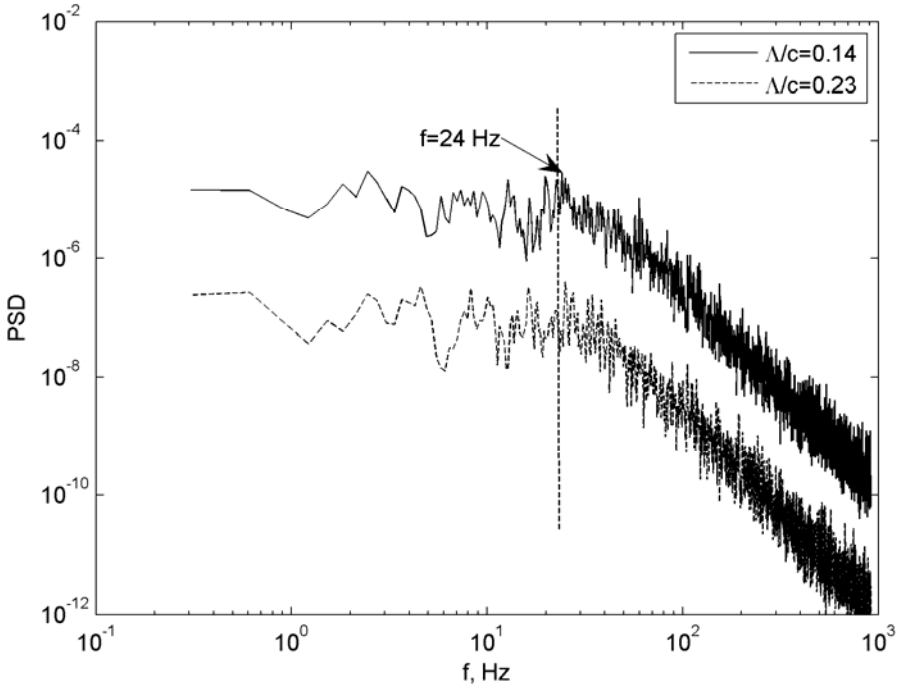

e)

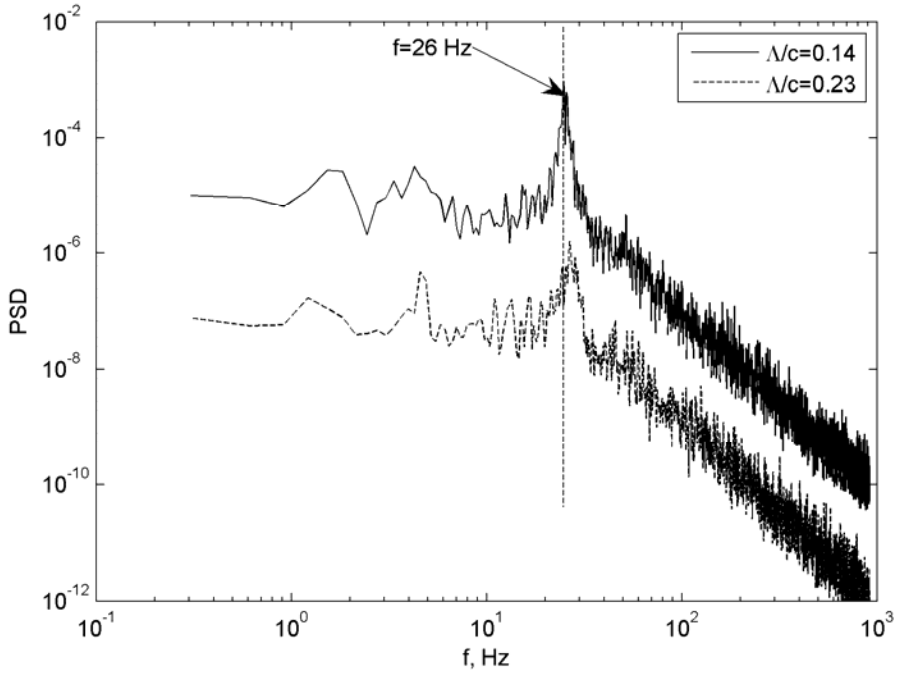

f)

Fig. 3.8 Comparison of PSD with independent change in integral length scale from Λ=0.14 to 0.23. a) α=18 deg and b) α=20 deg for *Re*=55,000, c) α=20 deg and d) α=23 deg for *Re*=75,000, e) α=21 deg and f) α=23 for *Re*=100,000.

At Tu=9.5% (Fig. 3.9), the velocity profiles are examined at α=20 deg for all Reynolds numbers with increasing Λ/c=0.08 to 0.14 (Λ=12 to 21 mm). For Re=55,000 and Λ/c=0.08 (Fig. 3.9a), the maximum velocity deficit is 0.32 occurring around y/c=-0.125. The upper part of the velocity profile does not have a smooth transition from outer wake to center wake, whereas the shape of the lower part is smoother. At Λ/c=0.14, the wake profile is seen to skew downwards, with decreased velocity deficits. The width of the wake is narrower comparing to the ones formed under large free-stream integral length scale, and it appears to skew to the negative side of the y-axis. At Re=75,000 (Fig. 3.9b) and Re=100,000 (Fig. 3.9c) the wake profiles also skew downwards and become narrower with increasing Λ/c. This is contrary to the observation at Tu=4.1%, where the wakes grow wider when increasing integral length scale. Obviously the wake is suppressed when Λ/c increases from 0.08 to 0.014. In fact, the general shape is similar to the independent change of the turbulence intensity featuring a downward shift of the upper part of the wake and the maximum velocity deficit. Differences in velocity deficit below y/c=-0.75 are also obvious, where large velocity deficit appears as the integral length scale increases.

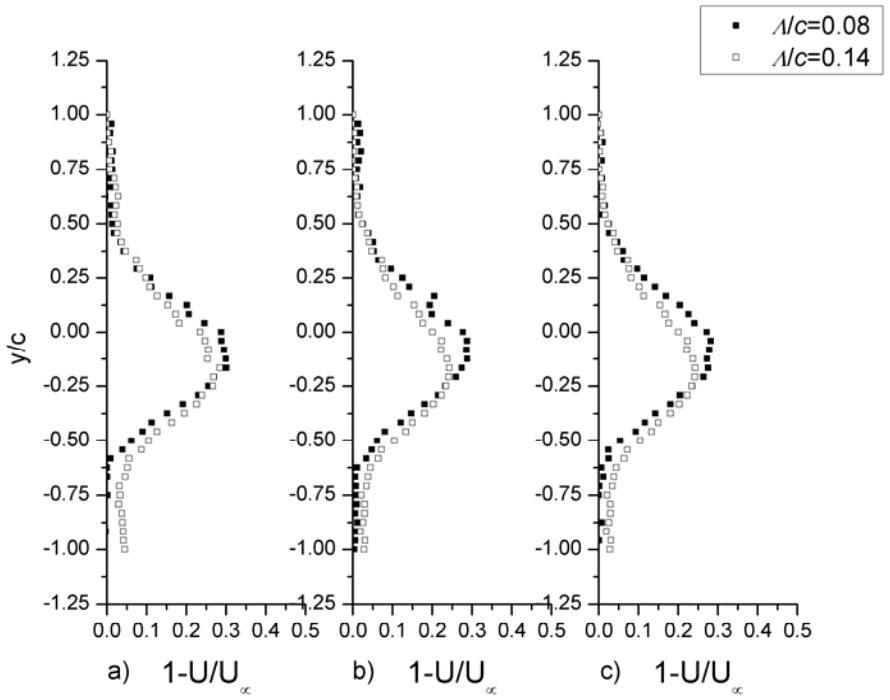

Fig. 3.9 Comparison of velocity deficits at constant *Tu*=9.5%, with *Λ/c*=0.08 and *Λ/c*=0.14. a) *Re*=55,000, b) *Re*=75,000, c) *Re*=100,000.

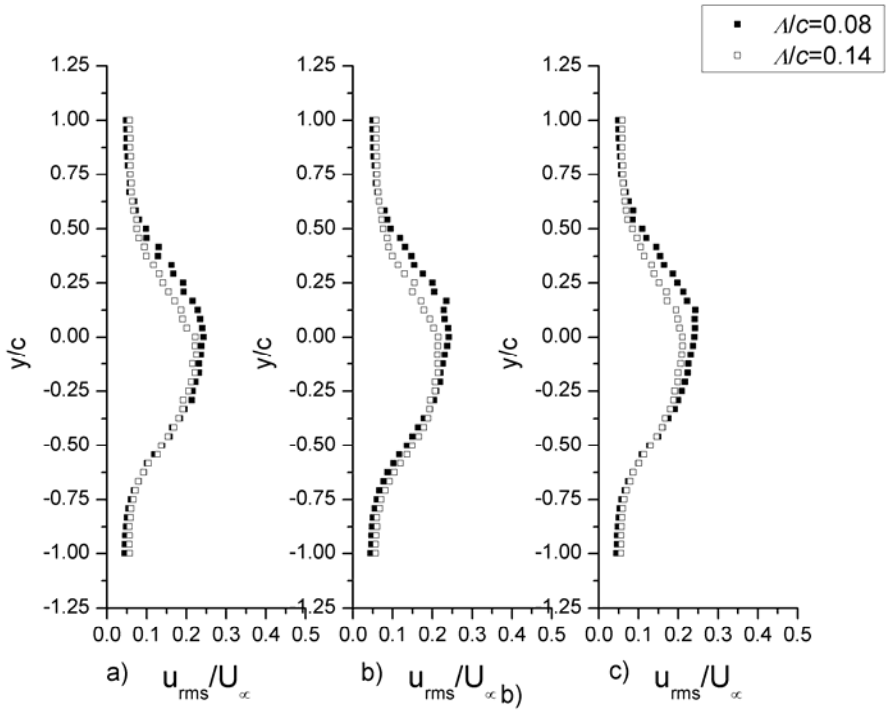

Fig. 3.10 Comparison of integral length scale effects at constant turbulence intensity *Tu*=9.5% with *Λ/c*=0.08 and *Λ/c*=0.14. a) *Re*=55,000, b) *Re*=75,000, c) *Re*=100,000.

The differences in the turbulence intensity profiles are obvious at the upper part of the wake (Fig. 3.10). An increase in integral length scale results a decrease in wake turbulence level, thus the wakes appear narrower. It appears that the free-stream integral length scale have less impacts on the lower part of the wake.

Table 3.3 Independent effect of turbulence integral length scale at *Tu*=9.5%

	Free-stream condition	C_l	C_d
Re=55000, α= 20 deg	Λ/c=0.08	1.58	0.20
	Λ/c=0.14	1.59	0.21
Re=75000, α= 20 deg	Λ/c=0.08	1.59	0.23
	Λ/c=0.14	1.64	0.22
Re=100,000, α= 20 deg	Λ/c=0.08	1.58	0.23
	Λ/c=0.14	1.63	0.22

The coefficients of lift are slightly larger with higher (Table 3.3). Reduced drag is observed at *Re*=55,000 and 100,000 except at *Re*=75,000, but the differences are within uncertainty limits.

By observing the PSD at *Re*=55,000 (Fig. 3.11a), weak peaks are observed at *f*=20 Hz for both Λ/c=0.08 and 0.14 cases. With increasing the Reynolds number to 75,000 (Fig. 3.11b) and 100,000 (Fig. 3.11c), weak peaks are seen at *f*=26 and 36 Hz for Λ/c=0.08, and no peaks can be seen for Λ/c=0.14.

In general, with the increase in the integral length from Λ/c=0.08 to 0.14, a narrower wake, less intense frequency-centred activities and higher lift coefficient all imply the boundary layer is less separated from the airfoil. Although very subtle, it seems that the small size of the integral length scale do have effects on the post-stall angles of attack of the airfoil.

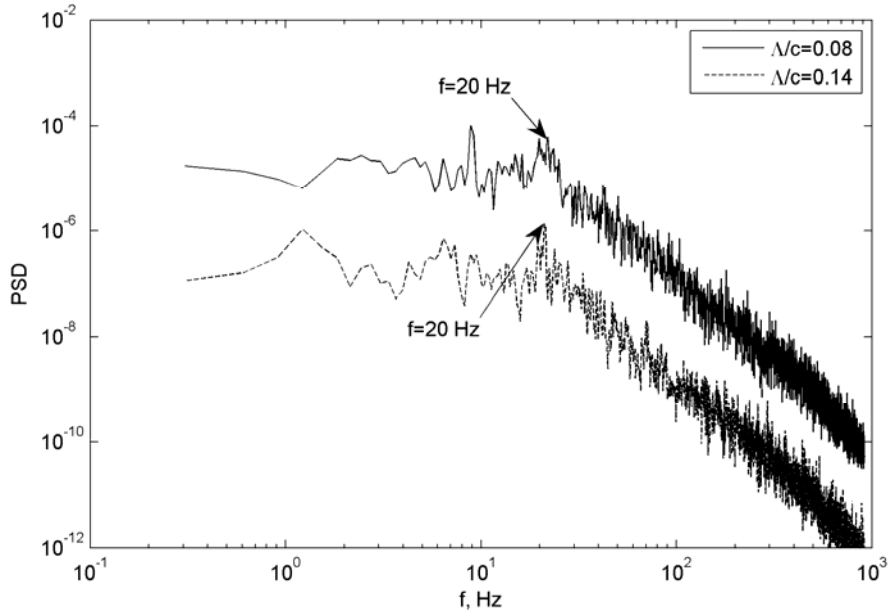

a)

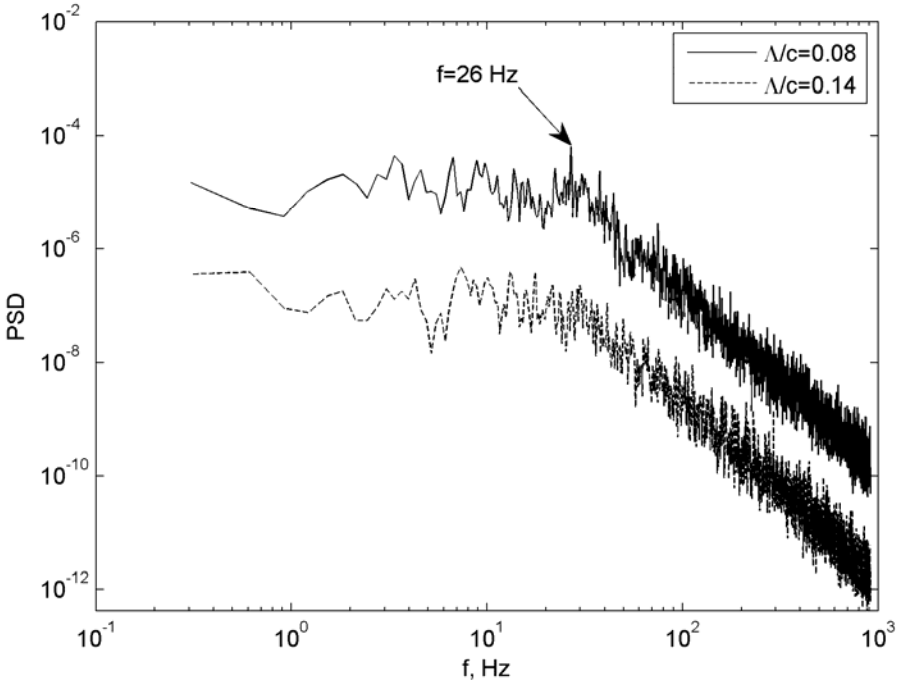

b)

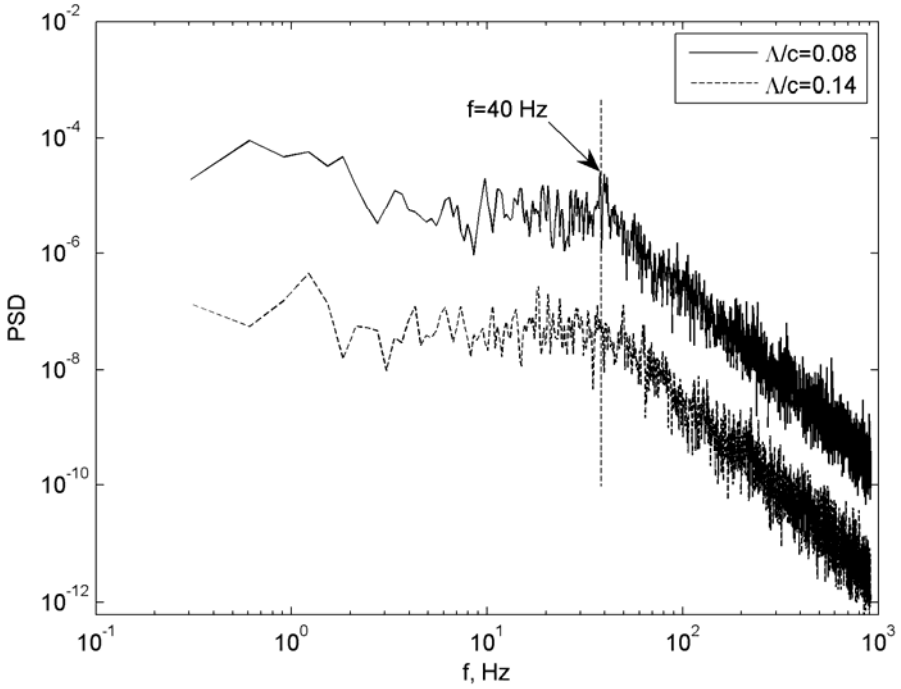

c)

Fig. 3.11 Comparison of PSD at constant turbulence intensity *Tu*=9.5% with *Λ/c*=0.08 and *Λ/c*=0.14. a) *Re*=55,000, b) *Re*=75,000, c) *Re*=100,000.

Conclusions

The independent effects of the turbulence intensity and the integral length scale on the wake structure of an asymmetric airfoil (S1223) have been investigated experimentally at three different Reynolds numbers Re=55,000, 75,000 and 100,000.

The independent effects of the turbulence intensity were examined in detail at Tu=4.1% and 9.5% with free-stream turbulence integral length scale fixed at Λ/c=0.14. The differences in the wake structure and corresponding lift and drag coefficient are prominent. Over the range of the Reynolds numbers tested, the upper and the middle part of the wake are greatly affected by the increasing the free-stream turbulence intensity. By increasing the free-stream turbulence intensity independently, the wake becomes narrower, and the velocity deficits and wake turbulence intensity decreases. Increased lift and reduced drag have also been observed. From PSD, the strength of the shedding vortices becomes less detectable as no frequency-centred peak is seen. Higher level of free-stream turbulence intensity has better capabilities to suppress the wake turbulence and vortex-shedding by means of increasing the momentum exchange between the outer flow and the wake. It reduces wake width and suppression of vortex-shedding show a sign of a delay trailing edge boundary layer separation. As a result the stall characteristic is less obvious as the increasing the high free-stream turbulence intensity slows down the process of the trailing edge separation.

The independent effects of the turbulence integral length scale were examined first at a constant 4% turbulence intensity. At certain stall angles of attack and increasing free-stream integral length scale from Λ/c=0.14 to Λ/c=0.23, the wake becomes wider and skew to the negative direction of y/c. Large increases in velocity deficits and turbulence integral length scale are evident at the middle and the lower part of the wake. The lift coefficient decreases, and the drag coefficient increases. Weak vortex-shedding phenomena are spotted at lower part of the wake (y/c=-0.5). The widened wake indicates the boundary layer separates earlier under the influence of the large integral length scale. However, the instability of the separated boundary lay can only initiate very weak vortex structure for both cases. By further increasing the angle of attack, the wakes for both cases grow wider, indicating a more separated boundary layer. The impact of the integral length scale is subtle as the width, velocity deficits, turbulence intensity in the wake are

nearly the same. The wake structures also behave similarly and strong vortex-shedding is captured in both cases.

At free-stream turbulence intensity Tu=9.5%. The velocity and turbulence intensity profiles skew to the negative y/c for all Reynolds numbers when the integral length increase from Λ/c=0.08 to Λ/c=0.14. However, the velocity deficits and wake turbulence are shown to decrease. Frequency-centered activities are very weak and can only be spotted at Λ/c=0.14. Although the lift coefficient is seen to increase at Λ/c=0.14, the difference in lift and drag coefficient are within uncertainty limits. In general the effect of current integral length scale under high turbulence is subtle.

References

[1] Farsimadan, E., and Mokhtarzadeh-Dehghan, M.R., "An experimental study of the turbulence quantities in the boundary layer and near-wake of an airfoil placed at upstream of a 90º bend," Exp. Therm. Fluid Sci, (2010), doi: 10.10 16/j.expthermflusci.2010.02.005

[2] Lissaman, P. B. S., "Low-Reynolds-Number Airfoils," Ann. Rev. Fluid Mech,1983, 15:223-39.

[3] Carmichael, B. H., "Low Reynolds Number Airfoil Survey," Vol. 1, 1981, NASA CR-165803.

[4] Mueller, T. J., and Batill, S. M., "Experimental Studies of Separation on a Two-Dimensional Airfoil at Low Reynolds Numbers," AIAA Journal, Vol. 20, No. 4, 1982, pp. 457-463

[5] Arena, A. V., and Muller, T. J., "Laminar Separation, Transition and Turbulent Reattachment near the Leading Edge of Airfoils," AIAA Journal, Vol. 18, No. 7, 1980, pp. 747-753

[6] Campbell, G. S., "Turbulence in the wake of a thin airfoil at low speeds," National Advisory Committee for Aeronautics, Technical memorandum 1427 (1957)

[7] Hah, C., and Lakshminarayana, B., "Measurement and prediction of mean velocity and turbulence structure in the near wake of an airfoil." Journal of Fluid Mechanics, Vol. 115, 1982, p251

[8] Huang, R., and Lin, C., "Vortex Shedding and Shear-Layer Instability of Wing at Low-Reynolds Numbers" AIAA Journal, Vol. 33, No. 8, 1995, pp. 1398-1403

[9] Yarusevych, S., Sullivan, P. E., and Kawall, J. G., "On vortex shedding from an airfoil in low-Reynolds-number flows" Journal of Fluids Mechanics, Vol. 632, 2009, pp. 245-271.

[10] Mueller, T. J., Prohlen, L. J., Conigliaro, P. E., and Jansen, B. J., "The Influence of Free-Stream Disturbances on Low Reynolds Number Airfoil Experiments," Experiments in Fluids, Vol. 1, 1983, pp. 3-14.

[11] Hoffmann, J. A., "Effects of Free-stream Turbulence on the Performance Characteristics of an Airfoil," AIAA Journal, Vol. 29, No. 9, 1991, pp. 1353-1354.

[12] Payne, F. M., and Nelson, R. C., "Aerodynamic Characteristics of and Airfoil in a Nonuniform Wind Profile," Journal of Aircraft, Vol. 22, No. 1, 1985, pp. 5-10.

[13] Devinant, Ph., Laverne, T., and Hureau, J., "Experimental study of wind-turbine airfoil aerodynamics in high turbulence," Journal of Wind Engineering and Industrial Aerodynamics, No. 90, 2002, pp. 689-707.

[14] Meier, H. U., and Kreplin, H. P., "Influence of Free-stream Turbulence on Boundary-Layer Development," AIAA Journal, Vol. 18, No. 1, 1980, pp. 11-15.

[15] Howard, R. H., and Kindelspire, D. W., "Free-stream Turbulence Effects on Airfoil Boundary-Layer Behavior at Low Reynolds Number," Journal of Aircraft, Vol. 27, No. 5, 1990, pp. 469-470.

[16] Huang, R. F., and Lee, H. W., "Turbulence Effect on Frequency Characteristics of Unsteady Motions in Wake of Wing," AIAA Journal, Vol. 38, No. 1, 2009, pp. 87-94.

[17] Zhang, Q., Lee, S. W., and Ligrani, P. M, "Effects of surface roughness and freestream turbulence on the wake turbulence structure of a symmetric airfoil," Physics of Fluids, June, 2004, pp. 2044-2053

[18] Howard, R. H., and Kindelspire, D. W., "Free-stream Turbulence Effects on Airfoil Boundary-Layer Behavior at Low Reynolds Number," Journal of Aircraft, Vol. 27, No. 5, 1990, pp. 469-470.

[19] Selig, M. S., and Guglielmo, J. J., "High-Lift Low Reynolds Number Airfoil Design," Journal of Aircraft, Vol. 34, No. 1, 1997, pp. 72-79.

[20] Liu, R., Ting, D. S-K., and Checkel, M. D., “Constant Reynolds number turbulence downstream of an orificed perforated plate,” Exp. Therm. Fluid Sci, No. 31, 2007, pp. 897-908.

[21] Liu, R., and Ting, D. S-K., “Turbulent Flow Downstream of a Perforated Plated: Sharp-Edged Orifice versus Finite-Thickness Holes,” Journal of Fluids Engineering, Vol. 129, 2007, pp. 1164-1171.

[22] Welch, P.D, "The Use of Fast Fourier Transform for the Estimation of Power Spectra: A Method Based on Time Averaging over Short, Modified Periodograms," IEEE Trans. Audio Electroacoustics, Vol. AU-15, 1967, pp.70-73.

CHAPTER 4. CONCLUDING REMARKS AND RECOMMENDATIONS

Concluding Remarks

The independent effects of turbulence intensity and turbulence integral length scale on a S1223 asymmetric airfoil at low Reynolds numbers have been examined in the thesis. The lift and drag coefficients were examined from α=-5 to 25 deg, and then the wake structure were investigated at certain post-stall angles of attack specifically.

The independent effects of high level turbulence intensity are prominent on the airfoil examined with constant integral length scale. By increasing the turbulence intensity less than 0.5% to 9.5%, the stall is significantly delayed to higher angles of attack. The velocity deficits and turbulence intensity are reduced. The strength of vortex-shedding is also decreased. The wake structure indicates the boundary layer separation is effectively suppressed by the high free-stream turbulence intensity.

The independent effects of the free-stream turbulence integral length scale were studied at 4.1% and 9.5% turbulence intensity level. At low turbulence intensity level, the airfoil shows a slight early-stall when the integral length scale is increased (from Λ/c=0.14 to 0.23). The lower lift and higher drag are seen at stall angles of attack. The wake becomes wider with higher velocity deficits and turbulence intensity. There is no clear sign on the formation of the vortex structure. At post-stall angles of attack, the integral length scale has very subtle impact on the force coefficient and wake structure. The high strength vortex-shedding phenomena are captured for both cases.

At higher turbulence intensity, the effects of increasing the integral length scale from Λ/c=0.08 to 0.14 are subtle. A slight decrease on the lift coefficient is seen at post-stall region. The velocity deficits and wake turbulence are shown to decrease. Frequency-centered activities are very weak can only be spotted at certain Reynolds number. In general the effect of current integral length scale under high turbulence is subtle.

Recommendations

The free-stream turbulence intensity and turbulence integral length can affect the performance and wake structure of an asymmetric S1223 airfoil at low Reynolds numbers. However, current study does not investigate the mechanism that makes the airfoil behave differently in different free-stream turbulence conditions: that is, the boundary layer

behaviours are still not clear. To further investigated the boundary layer behaviour, two feasible methods: 1) oil flow visualization and 2) surface pressure taps may be employed. With these techniques, the boundary layer separation bubble and its location can be measured, and these can help to explain the different performance of the airfoil under different turbulence conditions.

Wavelet analysis could be used to complement the Fourier spectral analysis as it can not only reveal the features in the frequency domain and also in the time domain.

APPENDICES

APPENDIX A. Uncertainty analysis of lift and drag coefficient

The uncertainty analysis of the lift and drag coefficients usually consists of two parts: a) estimation of systematic error *B* (bias error), b) estimation of random error *P* (precision error). The total uncertainty is the calculated determined by:

$$W = (B^2 + P^2)^{0.5} \tag{A-1}$$

The lift and drag coefficients can be expressed as:

$$C_l = \frac{L}{1/2\rho V_\infty{}^2 A} = \frac{\overline{F}_{y1} + \overline{F}_{y2}}{qA} \tag{A-2}$$

$$C_d = \frac{D}{1/2\rho V_\infty{}^2 A} = \frac{\overline{F}_{x1} + \overline{F}_{x2}}{qA} \tag{A-3}$$

where *L* and *D* measured lift or drag respectively and *q* is free-stream dynamic pressure which was measured directly in the experiment using pitot-static tube. The uncertainty of the planform area *A* is negligible as it is too small comparing to other parameters in the equation, so the systematic error is calculated as:

$$B_{c_l} = \left(\left[\frac{\partial C_l}{\partial F_{y1}} B_{F_{y1}} \right]^2 + \left[\frac{\partial C_l}{\partial F_{y2}} B_{F_{y2}} \right]^2 + \left[\frac{\partial C_l}{\partial q} B_q \right]^2 \right)^{0.5} \tag{A-4}$$

$$B_{c_d} = \left(\left[\frac{\partial C_l}{\partial F_{x1}} B_{F_{x1}} \right]^2 + \left[\frac{\partial C_l}{\partial F_{x2}} B_{F_{x2}} \right]^2 + \left[\frac{\partial C_l}{\partial q} B_q \right]^2 \right)^{0.5} \tag{A-5}$$

The lift and drag are calculated by adding the time averaged force components from the load cells at each side of the airfoil. Samples *N*=20,000 of force data are collected over 20-sec duration; thus, the precision error of the forces with 95% confidence level can be expressed as:

$$P_{\overline{F}} = 2S_{\overline{F}} = \frac{2S_F}{\sqrt{N}} \tag{A-6}$$

Accordingly the precision errors of the lift and drag coefficient can be written as:

$$P_{c_l} = \left(\left[\frac{\partial C_l}{\partial F_{y1}} P_{F_{y1}} \right]^2 + \left[\frac{\partial C_l}{\partial F_{y2}} P_{F_{y2}} \right]^2 + \left[\frac{\partial C_l}{\partial q} P_q \right]^2 \right)^{0.5} \quad \text{(A-7)}$$

$$P_{c_d} = \left(\left[\frac{\partial C_d}{\partial F_{x1}} P_{F_{x1}} \right]^2 + \left[\frac{\partial C_d}{\partial F_{x2}} P_{F_{x2}} \right]^2 + \left[\frac{\partial C_d}{\partial q} P_q \right]^2 \right)^{0.5} \quad \text{(A-8)}$$

The systematic error is neglected in the uncertainty analysis because the experiment is a comparative test. The sample calculations of the lift coefficient uncertainty at α=-5 deg with the free-stream turbulence condition Tu=4.1%, Λ=11 mm, and Re=55000 are listed below:

$\bar{F}_{y1} = 0.442349$ N

$\bar{F}_{y2} = 0.497045$ N

$q = 20$ Pa

$A = 0.1161$ m^2

$$C_l = \frac{(0.44239 + 0.497045)\text{ N}}{20\text{ Pa} \times 0.1161\text{ m}^2} = 0.4044$$

$S_{F_{y1}} = 0.068173$ N

$$P_{\bar{F}_{y1}} = \frac{2S_{F_{y1}}}{\sqrt{N}} = \frac{2 \times 0.068173}{\sqrt{20000}} = 4.821 \times 10^{-4}\text{ N}$$

$S_{F_{y2}} = 0.116734$ N

$$P_{\bar{F}_{y2}} = \frac{2S_{F_{y2}}}{\sqrt{N}} = \frac{2 \times 0.116734}{\sqrt{20000}} = 8.254 \times 10^{-4}\text{ N}$$

$P_q = 0.3$ Pa

$$P_{c_l} = \left(\left[\frac{\partial C_l}{\partial F_1} P_{F_1} \right]^2 + \left[\frac{\partial C_l}{\partial F_2} P_{F_2} \right]^2 + \left[\frac{\partial C_l}{\partial q} p_q \right]^2 \right)^{0.5}$$

$$P_{c_l} = \left(\left[0.21401(4.821 \times 10^{-4}) \right]^2 + \left[0.19046(8.254 \times 10^{-4}) \right]^2 + \left[-0.020223(0.6) \right]^2 \right)^{0.5}$$

$$P_{c_l} = 0.01214$$

$$W_{C_l} \approx P_{C_l}$$

$$\frac{W_{C_l}}{C_l} = \frac{0.01214}{0.4044} \approx 0.03 = 3\%$$

APPENDIX B. Determination of Taylor microscale

To determine the Taylor microscale, the methodology used is similar to what has been described by Belmabrouk and Michard [1]. The Taylor microscale is usually obtained by fitting the first few auto correlation coefficient points with a parabola. It can be expressed as:

$$\rho(r) = \rho_0 - \frac{r^2}{\lambda^2} \tag{B-1}$$

where r is the stream-wise distant between two points. Theoretically R_0 is 1, but it is less than one in practice.

Temporal auto-correlation function is first calculated. It is then transformed to spatial auto-correlation function based on the Taylor's frozen eddy hypothesis. The transformation provides a good match if $u_{rms}/U_{mean}<<1$ and the turbulence is close to isotropic. The general approach is described below:

1. Plot spatial auto-correlation coefficient ρ(r) versus r^2 so the parabolic relationship becomes linear.
2. Set an interval [r_{min}, r_{max}]
3. Linear equations can be obtained and expressed as $\rho(r)$ as a function of r^2 using least square fit. Taylor microscale is square-root of the value approximated at where ρ(r) =0
4. Increasing r_{max} and repeat step 3, a new Taylor scale is obtained. The repeated procedures terminate if the relative error of the Taylor microscale is higher 5%. (table)
5. The final Taylor microscale is determined by averaging the possible different values.

References

[1] Belmabrouk, H., and Michard, M., "Taylor length scale measurement by laser Doppler velocimetry," Experiments in Fluids, Vol. 25, 1998, pp. 69-76.

Table D.1 Effects of r_{max} on the Taylor microsclae, Plate 50.8 with Tu=9.5%, Λ=21 mm and V_∞=5.7m/s

r_{min} (mm)	r_{max} (mm)	λ(mm)	$\lvert\lambda - \lambda_{ave}\rvert/\lambda_{ave}$ (%)	R_0
0.065	0.13	4.46	0	0.998
0.065	0.20	4.61	1.7	0.998
0.065	0.26	4.58	0.7	0.998
0.065	0.33	4.61	0.9	0.998
0.065	0.39	4.65	1.4	0.998
0.065	0.46	4.67	1.6	0.998
0.065	0.52	4.71	2.0	0.998
0.065	0.58	4.75	2.5	0.998
0.065	0.65	4.78	2.9	0.998
0.065	0.72	4.83	3.4	0.998
0.065	0.78	4.87	4.0	0.998
0.065	0.85	4.92	4.6	0.998
0.065	0.91	4.97	5.2	0.998
		λ_{ave} =4.72		$R_{0,ave}$=0.998

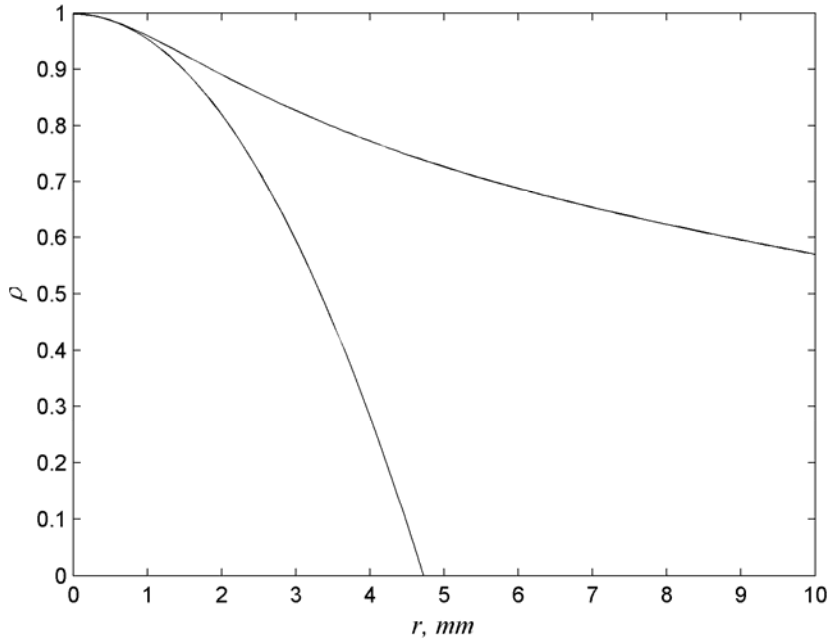

Fig.B. 1 Parabola determinded from the auto-correlation coefficient

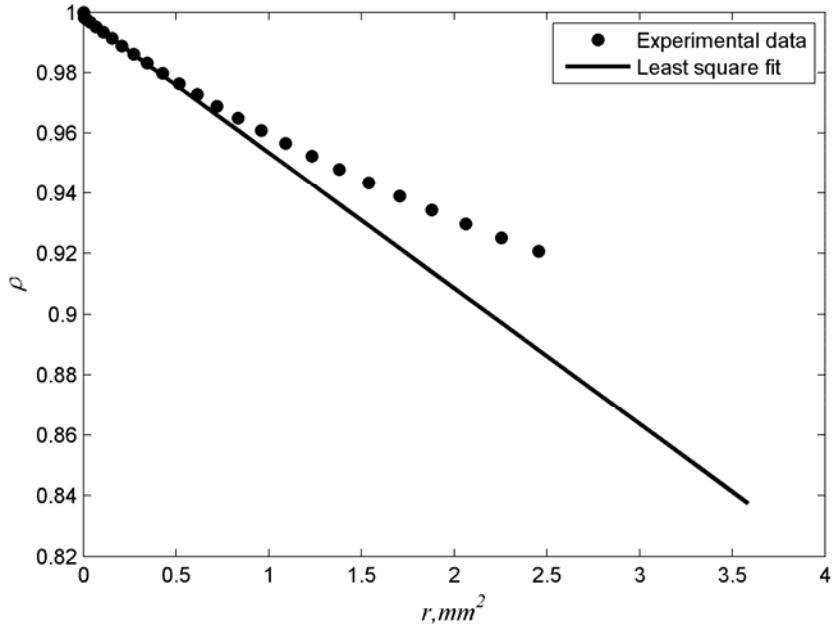

Fig.B. 2 Determination for Taylor microscale

APPENDIX C. On the assumption of Taylor's hypothesis

The integral length scale is calculated by integrating the spatial correlation function (two-point correlation function). For hot-wire measurement, it is easier to find temporal correlation function (auto-correlation function) than to find the spatial correlation function. The approximation of spatial correlations by temporal correlations is known as Taylor's Hypothesis [1]. And it is based on Eq (C-1). In grid turbulence with $u'/U_{mean}<<1$, it is quite accurate [2]. Hinze [3] also points out that the Taylor's hypothesis is based on the assumption of homogeneity of the flow field. For shear flow, validity of Taylor's hypothesis is less clear.

$$\frac{\partial}{\partial t} = u_i \frac{\partial}{\partial x_i} \tag{C-1}$$

References

[1] Tennekes, H., and Lumley, J. L., *A First Course in Turbulence*, 1st ed, The MIT Press, Massachusetts, 1972,

[2] Pope, S. B., *Turbulent Flow*, 1st ed, Cambridge University Press., Cambridge, 2000,

[3] Hinze, J. O., *Turbulence*, 2nd ed, McGraw-Hill , New York, 1975

APPENDIX D. Comparison of the results to literature

Fig.D. 1 shows the comparison of the lift coefficients obtained based on the current setup and published data [1] at Re=50,000 (Fig.D. 1a) with clean installation (i.e. no perforated plate was installed). The lift coefficient of current study is larger comparing to the published data before the airfoil stalls at α=4 deg. It can also be observed that the lift coefficient of the current study is lower starting from α<13 deg. At Re=100,000 (Fig.D. 1b), the current study agrees the Selig data at pre-stall region. However, it has earlier stall at α=6 deg and a lower maximum lift coefficient. The lift in post-stall region is also lower than what has been recorded by Selig. At Re=150,000 (Fig.D. 1c), good agreement is observed at pre-stall region (α<15 deg). The current airfoil is still features an earlier stall and a lower lift coefficient at post-stall angles of attack (α>20 deg).

Fig.D. 2 illustrates the drag coefficient at Re=100,000 (Fig.D. 2a) and Re=150,000 (Fig.D. 2b). It should be noted that the drag data by Selig is estimated through wake survey, whereas the drag of the current study is measured directly using force transducer, so direct comparison is less meaningful.

The turbulence intensity of the clean wind tunnel around 0.5% is considered a little high. However the largest contribution to the difference in the data is believed to be the uncertainty of the airfoil. The profile the wooden airfoil has discrepancy to the original profile which may change the airfoil performance.

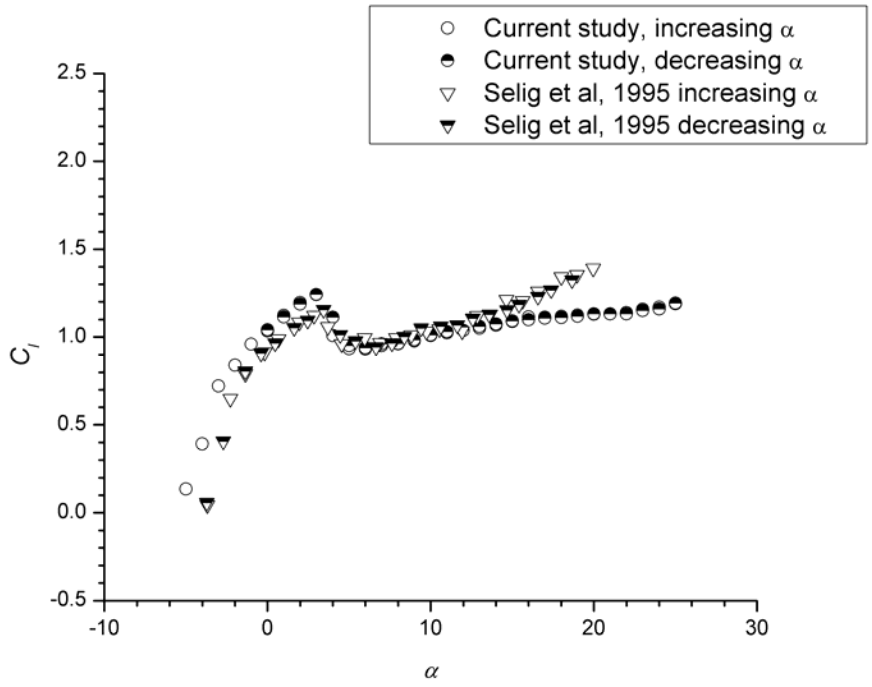
Current study, increasing α
Current study, decreasing α
Selig et al, 1995 increasing α
Selig et al, 1995 decreasing α
C_l
α
2.5
2.0
1.5
1.0
0.5
0.0
-0.5
-10
0
10
20
30

a)

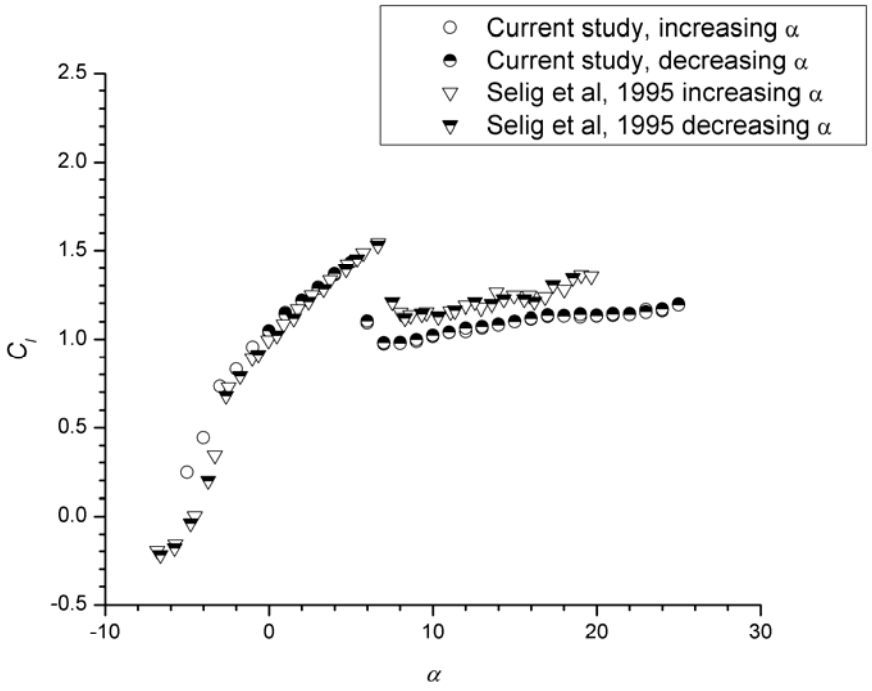
Current study, increasing α
Current study, decreasing α
Selig et al, 1995 increasing α
Selig et al, 1995 decreasing α
C_l
α
2.5
2.0
1.5
1.0
0.5
0.0
-0.5
-10
0
10
20
30

b)

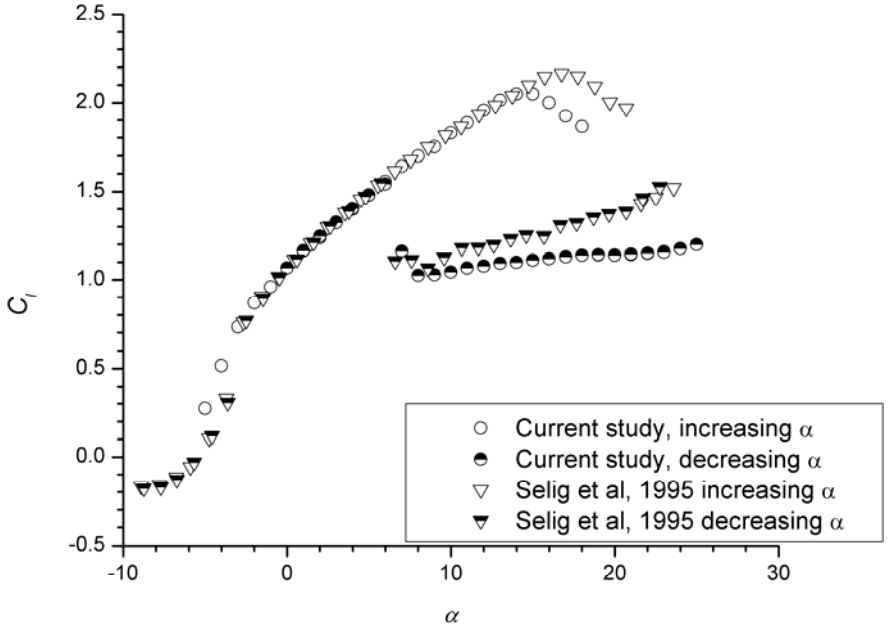

c)

Fig.D. 1 Comparison of current lift data with published literature. a) *Re*=50,000, b) *Re*=100,000, c) *Re*=150,000.

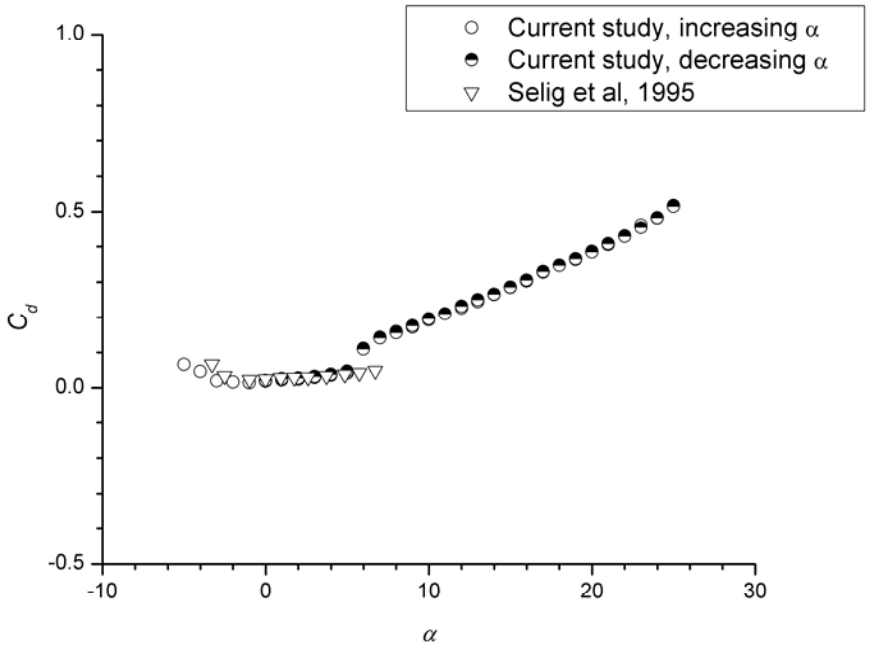

a)

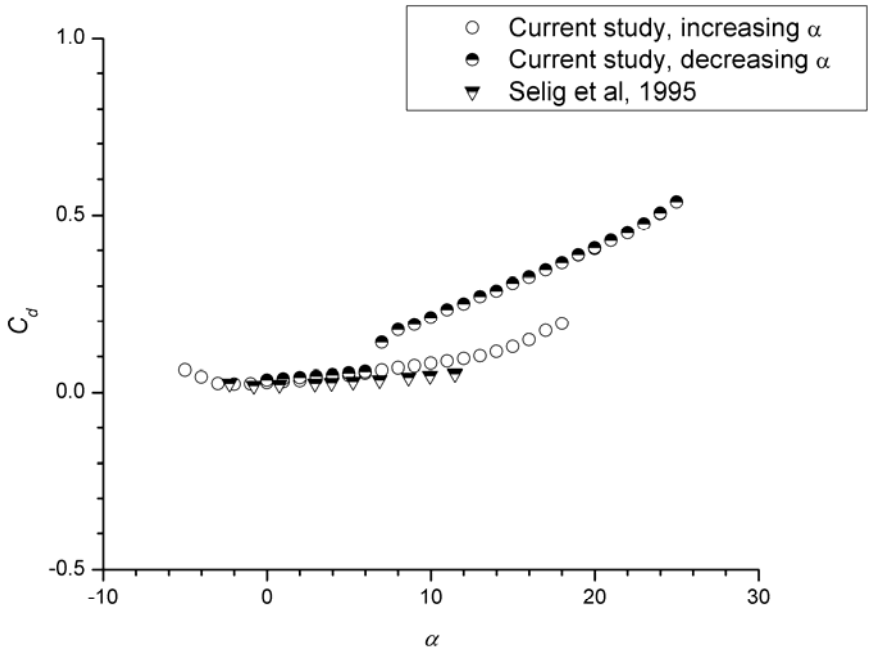

b)

Fig.D. 2 Comparison of current drag data with published literature. a) *Re*=50,000, b) *Re*=100,000, c) *Re*=150,000.

Reference

[1] Selig, M. S., Guglielmo, J. J., Broeren, A. P., and Giguere, P., "Summary of Low-Speed Airfoil Data," Vol. 1, SoarTech Publications, Virginia Beach, VA, 1995.

APPENDIX E. Comments on straining rate effects

The mean turbulence straining rate (rate of strain) is also a useful parameter in turbulence study. It comes to a question whether the straining rate of the turbulence is a more effective measuring parameter other than turbulence intensity and turbulence integral length scale, as it takes into account both the fluctuation and the scale of the turbulence simultaneously. The turbulence straining rate is defined as u'/λ, where u' is the root mean square turbulent fluctuation intensity and λ is the Taylor microscale. It is easily seen that large straining rate means the turbulence fluctuation plays a dominant role, and the small straining rate means the turbulence scale has more effects.

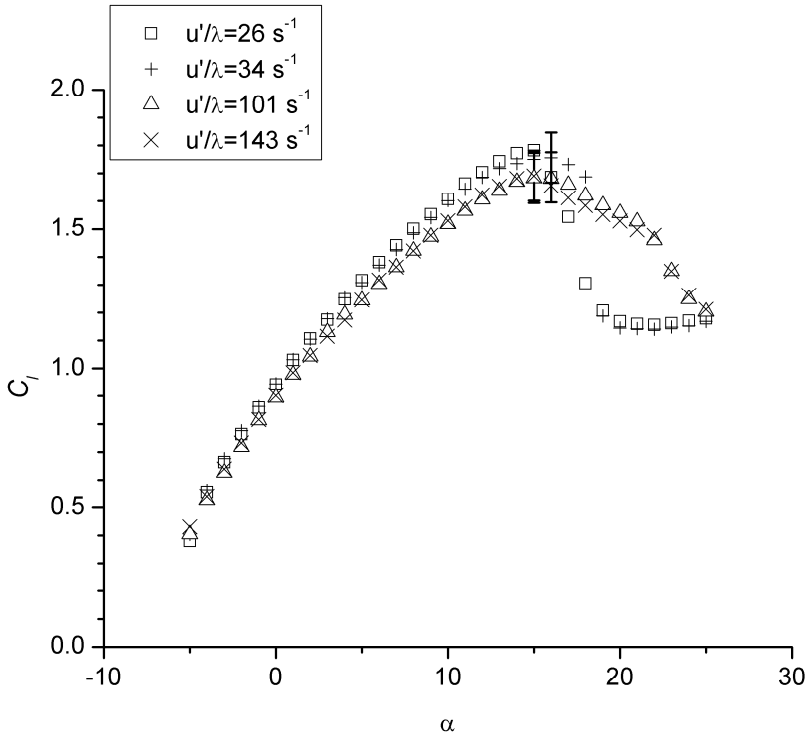

Fig.E. 1 Straining rate effects on the lift coefficient of S1223 at *Re*=55,000.

APPENDIX F. Uncertainty analysis of Reynolds number

The Reynolds number is defined as:

$$\mathrm{Re} = \frac{\rho U_{mean} c}{\mu} \tag{F-1}$$

Base on ideal gas law, the density is expressed in:

$$\rho = \frac{P_{atm}}{RT} \tag{F-2}$$

If we can express the mean free-stream velocity in terms of the free-stream dynamic pressure, then Equation (F-1) becomes:

$$\mathrm{Re} = a\left(\frac{qP_{atm}}{T}\right)^{0.5} \tag{F-3}$$

where a is a constant if the uncertainty of chord and viscosity is negligible:

$$a = \frac{\sqrt{2}c}{\mu\sqrt{R}} \tag{F-4}$$

Where R is Universal gas constant of 287.058 J/Kg·K, and μ is the kinematic viscosity of $1.827(10)^{-5}$ Pa·s.

As a result, the Reynolds number is simplified to be a function of the free-stream dynamic pressure q, atmospheric pressure P_{atm}, and the temperature T inside the wind tunnel.

The free-stream dynamic pressure was monitored by a Dwyer 475 with 1.5% accuracy in full scale (0.249 Pa). It was also noticed that the fluctuation of the flow during the experiment is ±3 Pa. The atmospheric pressure was measured using a Kestrel Meters with an accuracy of 170 Pa (0.05 inHg). The fluctuation of the atmospheric pressure was estimated to be ±200 Pa. The temperature was measured by Barnant Thermometer with an accuracy of 0.7 K. The temperature fluctuation was ±3 K. The estimated errors above are all based on 95% confidence level.

The uncertainty of the Reynolds number consists of bias and precision error:

$$W_{\mathrm{Re}} = \left(B_{\mathrm{Re}}{}^2 + P_{\mathrm{Re}}{}^2\right)^{0.5} \tag{F-5}$$

$$B_{\mathrm{Re}} = \left[\left(\frac{\partial \mathrm{Re}}{\partial q} B_q\right)^2 + \left(\frac{\partial \mathrm{Re}}{\partial P_{atm}} B_{P_{atm}}\right)^2 + \left(\frac{\partial \mathrm{Re}}{\partial T} B_T\right)^2\right]^{0.5} \tag{F-6}$$

$$P_{\mathrm{Re}} = \left[\left(\frac{\partial \mathrm{Re}}{\partial q} P_q \right)^2 + \left(\frac{\partial \mathrm{Re}}{\partial P_{atm}} P_{P_{atm}} \right)^2 + \left(\frac{\partial \mathrm{Re}}{\partial T} B_T \right)^2 \right]^{0.5} \tag{F-7}$$

where:

$$\frac{\partial \mathrm{Re}}{\partial P_{atm}} = 0.5a \left(\frac{qP_{atm}}{T} \right)^{-0.5} \frac{q}{T} \tag{F-8}$$

$$\frac{\partial \mathrm{Re}}{\partial q} = 0.5a \left(\frac{qP_{atm}}{T} \right)^{-0.5} \frac{P_{atm}}{T} \tag{F-9}$$

$$\frac{\partial \mathrm{Re}}{\partial T} = 0.5a \left(\frac{qP_{atm}}{T} \right)^{-0.5} \left(\frac{-qP_{atm}}{T^2} \right) \tag{F-10}$$

The sample of calculations is listed below at P_{dyn}=64 Pa, P_{atm}=98990 Pa, and T=300 K.

$$\begin{aligned} B_{\mathrm{Re}} &= \left[\left(\frac{\partial \mathrm{Re}}{\partial q} B_q \right)^2 + \left(\frac{\partial \mathrm{Re}}{\partial P_{atm}} B_{P_{atm}} \right)^2 + \left(\frac{\partial \mathrm{Re}}{\partial T} B_T \right)^2 \right]^{0.5} \\ &= 0.5(695) \left[\left(2.271(3.735) \right)^2 + \left(0.001468(170) \right)^2 + \left(-0.4844(0.7) \right)^2 \right]^{0.5} \\ &\approx 2950 \end{aligned}$$

$$\begin{aligned} P_{\mathrm{Re}} &= \left[\left(\frac{\partial \mathrm{Re}}{\partial q} P_q \right)^2 + \left(\frac{\partial \mathrm{Re}}{\partial P_{atm}} P_{P_{atm}} \right)^2 + \left(\frac{\partial \mathrm{Re}}{\partial T} P_T \right)^2 \right]^{0.5} \\ &= 0.5(695) \left[\left(2.271(3) \right)^2 + \left(0.001468(200) \right)^2 + \left(-0.4844(3) \right)^2 \right]^{0.5} \\ &\approx 2420 \end{aligned}$$

$$\begin{aligned} W_{\mathrm{Re}} &= (B_{\mathrm{Re}}{}^2 + P_{\mathrm{Re}}{}^2)^{0.5} \\ &= (2950^2 + 2420^2)^{0.5} \\ &\approx 3800 \end{aligned}$$

At Re=100,000, the uncertainty is ±3800 (±3.8%) with 95 % confidence level

VITA AUCTORIS

Ning Cao was born in 1982 in Beijing, China, P. R. After graduating from Beijing 101 middle school, he attended Beijing Institute of Technology and got his diploma in Electronic Information Technology. In 2008, he graduated from Lakehead University with a Bachelor of Engineering degree with first class honours in Mechanical Engineering. He is currently a candidate of the Master of Applied Science in Mechanical Engineering at the University of Windsor.